Neutron scattering from the Heisenberg ferromagnets EuO and EuS. III. Spin dynamics of EuO†

O. W. Dietrich* and J. Als-Nielsen*
Research Establishment Risø, DK 4000 Roskilde, Denmark

L. Passell
Brookhaven National Laboratory, Upton, New York 11973
(Received 13 May 1976)

Inelastic neutron scattering has been used to investigate the spin dynamics of the isotropic Heisenberg ferromagnet EuO over a wide range of wave vectors and over a temperature range extending from 0.14 to $1.9\,T_C$. Below the ordering temperature spin-wave renormalization is found to agree well with the predictions of Dyson-Maleev theory (including the dynamical but not the kinematical interaction) when both exchange and dipolar couplings between the Eu^{2+} ions are taken into account. At temperatures near T_C broadening of the spin-wave lines was observed. For hydrodynamic spin waves, the wave-vector dependence of the linewidths is found to be consistent with the expectations of microscopic spin-wave theory and the temperature dependence with predictions based on dynamical scaling. At T_C, linewidths were found to deviate from the $q^{5/2}$ wave-vector dependence expected on the basis of dynamical scaling arguments when only exchange couplings are taken into consideration. But when dynamical scaling theory is modified by including dipolar interactions, it satisfactorily accounts for the weaker q dependence observed experimentally. Current microscopic theories appear to overestimate the magnitudes of the linewidths at T_C although above T_C theory properly predicts the temperature dependence of the spin diffusion coefficient in the hydrodynamic regime and also provides a good estimate of its magnitude.

I. INTRODUCTION

In the first two papers of this series we were concerned with neutron scattering studies of the exchange constants and static critical properties of EuO and EuS. In this paper our attention will be directed to the application of inelastic-neutron-scattering methods to the study of the spin dynamics of EuO. The experiments to be described were planned with the idea of providing as complete a view as possible of spin motions in EuO over the widest practical span of wave vectors and over a broad temperature range extending from the low-temperature ordered phase, in which spin-wave modes predominate, through the critical regime to the high-temperature disordered phase in which spin motion becomes primarily diffusive in character. Attention was concentrated on EuO alone because the magnetic couplings are strongest in this material and the details of its dynamic behavior are therefore easier to resolve experimentally.

It is generally accepted that inelastic neutron scattering is the most direct way to study magnetic spin dynamics on a microscopic scale and, in fact, magnets of almost every description have been investigated with neutrons. To mention a few representative examples, there are data in the literature on $RbMnF_3$,[1,2] an isotropic Heisenberg antiferromagnet, on the isotropic metallic ferromagnets Fe,[3-5] Co,[6] and Ni,[7,8] and on the anisotropic Heisenberg ferromagnets $CrBr_3$,[9] and MnP.[10] But as far as the isotropic Heisenberg ferromagnets EuO and EuS are concerned, very little information is available beyond that contained in preliminary accounts of our measurements.[11,12] As was noted in paper I, this is because neutron scattering is difficult in materials as strongly absorbing as europium. To the best of our knowledge, the data to be reported here thus represent the first reasonably complete and systematic set of experimental observations of the spin dynamics of an isotropic exchange-coupled ferromagnetic system.

This system has long been regarded as nearly ideal from the viewpoint of theory and much effort has consequently been devoted to models describing its static and dynamic behavior. For dynamics in the spin-wave regime below the ordering temperature T_C, probably the most comprehensive of the available theoretical treatments is that of Vaks, Larkin, and Pikin[13] but many others have been presented. Readers will find references to earlier work on this subject in the papers of Vaks *et al.* and a complete review of work previous to 1966 in Keffer's monograph on spin-wave theory.[14] Above T_C, in the spin-diffusion regime, there is also an extensive literature. de Gennes,[15] Mori and Kawasaki,[16] and Bennett and Martin[17] have done work of particular relevance to the questions of interest here, but many others have made important contributions. An excellent summary and critique of the current theory can be found in the recent article of Månson and Sjöl-

lander,[18] which also contains references to the earlier literature.

Although the spin-wave and spin-diffusion theories are generally considered to be successful, they do not provide satisfactory descriptions of experimental observations near T_C. While such difficulties were not entirely unexpected when the theories were originally proposed, their full significances was not appreciated until relatively recently when Halperin and Hohenberg[19] extended the static scaling ideas developed by Widom[20] and Kadanoff[21] to critical spin dynamics. As formulated by Halperin and Hohenberg, dynamical scaling retains the basic assumption of static scaling, namely, that the spin correlation range κ_1^{-1} defines a natural length scale. This assumption, Halperin and Hohenberg point out, carries with it the implication that dynamical behavior in the hydrodynamic regime, where the wave vector $\vec{q}$ is small compared to κ_1, can be expected to be different from behavior in the critical regime where $\vec{q}$ is large compared to κ_1. Consequently, it should not be surprising to find that theories which are basically hydrodynamic in character, such as the spin-wave and spin-diffusion models of magnetic dynamics, do not apply equally well to the critical regime near T_C.

Besides clarifying the distinction between hydrodynamic and critical theories, Halperin and Hohenberg also showed that dynamical scaling implies that the characteristic (half-area) frequency $\hat{\omega}_q(\kappa_1)$ of the spectral weight function $F(q, \omega)$ (defined in Sec. II of paper II) can be expressed as q^u times a scaling function $\Omega(\kappa_1/q)$ with the scaling exponent u having a value of $\frac{5}{2}$ for the isotropic ferromagnet. Subsequently, Résibois and Piette[22] calculated the normalized scaling function $\Omega(\kappa_1/q)/\Omega(0)$ for both the isotropic ferromagnet and antiferromagnet above T_C. Thus, even though dynamical scaling analysis does not give the actual form of $F(q, \omega)$, it does indicate how the half-area frequency of the spectral weight function can be expected to vary in the paramagnetic regime.

To carry the theory beyond this point has not been an easy matter. Above T_C, the greatest progress has been made by Hubbard[23] who developed a theory of spin correlations which provides a formalism for calculating the shape of $F(q, \omega)$ that is presumed to be valid for all values of κ_1/q. Nothing comparable can be done at present below T_C although the above-mentioned work of Vaks *et al.* does give a prescription for calculating $F(q, \omega)$ outside the critical regime. We will have more to say about these theories at a later stage.

But before proceeding to detailed discussions it may be helpful if we outline the organization of the text to follow. In Sec. II, it is our intention to summarize the main conclusions of dynamical theory to give the reader a theoretical perspective against which to view our experimental observations. This will be followed in Sec. III by a brief description of the experimental method. In Sec. IV the data analysis will be reviewed and in Sec. V the experimental results presented. Finally, Sec. VI will be devoted to a discussion of comparisons between theory and experiment and to the conclusions to be drawn from our observations.

II. THEORY

The magnetic inelastic-neutron-scattering cross section is basically determined by the dynamic structure factor $S(\vec{q}, \omega)$ as we noted in Sec. II of paper II. It was also remarked there that this factor can be expressed as the product of a static wave-vector-dependent susceptibility $\chi_{\vec{q}}$ and a normalized spectral weight function $F(q, \omega)$, the latter describing the dynamic response of the system. Previously, our attention was focused on the susceptibility $\chi_{\vec{q}}$; here by contrast we are interested in spin dynamics and the spectral weight function $F(q, \omega)$ will consequently become our primary concern.

Earlier we remarked that there is a large body of theory describing the dynamical behavior of Heisenberg magnets. Since space does not permit us to attempt to reproduce it in any detail here, we will be content simply to outline those parts of the theory which relate to our experiments and to quote without proof the formulas of interest. Those unfamiliar with the expressions cited will find complete derivations in the papers mentioned in this and Sec. I which also contain references to related literature.

But before attempting to summarize the theory, it may be helpful if we first make a few general remarks about the form our discussion will take. In the magnetically ordered regime below T_C, theory leads us to expect that spin fluctuations along and transverse to the direction of spontaneous magnetization will be quite different in character. Therefore, below T_C it will be necessary for us to discuss separately the longitudinal and transverse components of $F(q, \omega)$. At and above T_C, however, it is assumed that the absence of long-range magnetic order makes such distinctions meaningless, and we will consequently consider $F(q, \omega)$ to have the same form irrespective of any locally defined direction. Furthermore, since dynamical scaling implies that differences in dynamical response can be expected in the critical and hydrodynamic regimes, each will be treated separately. Nevertheless, it should

be borne in mind that the borderline between these regimes is broad and ill defined, and dynamical behavior is actually expected to change slowly and continuously as the transition from $q \ll \kappa_1$ to $q \gg \kappa_1$ takes place.

We might also note that we will not attempt to discuss in this section the influence of dipolar interactions on dynamical behavior. When such effects are known to be important, however, they will be included in the data analysis and specific mention of them made at that time.

A. $T < T_C$: Hydrodynamic regime

1. Transverse spin fluctuations

In the hydrodynamic regime below T_C the transverse spin fluctuations are the familiar spin waves discussed at length in paper I. There, the emphasis was on the use of low-temperature measurements of spin-wave dispersion to determine the magnitudes of the exchange couplings between spins. Here, by contrast, we will be concerned with the influence of increasing temperature on the energies and lifetimes of the excitations.

The theory of spin waves in magnetic systems at finite temperatures originated with the work of Dyson[24] whose approach to the problem involved the use of what is now called the Dyson-Maleev[25] transformation. Considering only the exchange interactions, Dyson rewrote the nearest-neighbor (nn) Heisenberg Hamiltonian

$$\mathcal{H} = -J_1 \sum_{\vec{n},\vec{n}+\vec{\rho}} \vec{S}_{\vec{n}} \cdot \vec{S}_{\vec{n}+\vec{\rho}}$$

in terms of the spin operators S^z and $S^{\pm}$, which he defined in terms of the Bose operators $a^\dagger$ and a. After Fourier transforming the Bose operators, the resulting Hamiltonian reduced to a term containing products of two operators and a term involving products of four operators of the form $a^\dagger_{\vec{q}_1} a^\dagger_{\vec{q}_2} a_{\vec{q}_3} a_{\vec{q}_4}$, the first representing the noninteracting spin waves and the second the interaction between them. To obtain linear equations of motion, Dyson decoupled the four operator products into products of two operators times a thermal average, i.e., into terms of the form $\langle a^\dagger_{\vec{q}_1} a_{\vec{q}_3} \rangle a^\dagger_{\vec{q}_2} a_{\vec{q}_4}$. From these equations he then found an equation for the spin-wave energies $\hbar\omega_{\vec{q}}(T)$ which can be put in the form (see, for example, Marshall and Lovesey[26] pp. 264–267)

$$\hbar\omega_{\vec{q}}(T) = 2zSJ_1[1 - C(T)/S](1 - \gamma_{\vec{q}}) , \tag{1}$$

where

$$C(T) = N^{-1} \sum_{\vec{q}} (1 - \gamma_{\vec{q}}) n_{\vec{q}} , \tag{2}$$

$$n_{\vec{q}} = [\exp(\hbar\omega_{\vec{q}}/kT) - 1]^{-1} ,$$

and

$$\gamma_{\vec{q}} = z^{-1} \sum_{\vec{r}} \exp(i\vec{q}\cdot\vec{r}) , \tag{3}$$

the summation in the last expression being over the vectors $\vec{r}$ from a given magnetic ion to its z nearest neighbors. Spin-wave energies are calculated by introducing the spin-wave spectrum at $T = 0$ K (see Section IV of paper I) into Eq. (2), computing $\gamma_{\vec{q}}$ from Eq. (3) and thence $\hbar\omega_{\vec{q}}(T)$ from Eq. (1), and then iterating until a self-consistent result is obtained.

There are two approximations in this theory. First, the Dyson-Maleev transformation is not exact since the Bose operators have an infinite spectrum, whereas there can be at most $2S$ spin deviations at a site with spin S. This is referred to in the literature as the "kinematic interaction" and is a rather small effect in EuO because the Eu^{2+} ion has the relatively large spin of $\frac{7}{2}$. Second, there is the so-called "dynamical interaction" which arises out of the approximation used to decouple the products of the Bose operators. The error introduced by decoupling is difficult to estimate from Dyson's work, but Keffer and Loudin[27] have derived the same equations from a more transparent physical model and they find them to be exact to second order in $C(T)/S$ or, in other words, to be correct in the limit when $[C(T)/S]^3 \ll 1$.

It is evident from the form of Eq. (1) that J_1 is renormalized by the temperature-dependent factor $1 - C(T)/S$ and that the quantity $J_1(T) = J_1[1 - C(T)/S]$ can be regarded as a renormalized exchange constant. In cubic lattices it is customary (in the limit of small q) to express spin-wave energies in ferromagnets by means of the relation $\hbar\omega = Dq^2$, where the stiffness constant $D = 2a^2SJ_1$ and a is the lattice constant, i.e., the cube edge in the fcc lattice. It follows from the theory outlined above that this relationship holds at all temperatures provided D is replaced by the renormalized stiffness constant $D(T) = 2a^2SJ_1(T)$.

Including the next-nearest-neighbor (nnn) interactions in the Hamiltonian introduces into the theory a next-nearest-neighbor exchange constant J_2 which is renormalized by a temperature-dependent factor of the form $1 - C'(T)/S$. Again

$$C'(T) = N^{-1} \sum_{\vec{q}} (1 - \gamma'_{\vec{q}}) n_{\vec{q}}$$

and

$$\gamma'_{\vec{q}} = z'^{-1} \sum_{\vec{r}} \exp(i\vec{q}\cdot\vec{r}') ,$$

the summation in the latter quantity is over the vectors $\vec{r}'$ from a given ion to the next-nearest-

neighbor positions. For the fcc magnetic lattice of EuO, the renormalized stiffness constant with both nearest- and next-nearest-neighbor exchange taken into account assumes the form $D(T) = 2a^2S[J_1(T)+J_2(T)]$. Figure 1 shows the renormalized exchange constants $J_1(T)$ and $J_2(T)$ for EuO calculated from the theory.

Dyson's approach gives us the excitation energies at finite temperatures but tells us nothing about spin-wave lifetimes; in fact the decoupling procedure he employed precludes the possibility of calculating the widths of the excitation peaks. Other methods can be used to obtain this information, however. For example, Cooke and Gersch,[28] Harris,[29] and Vaks *et al.*[13] have constructed microscopic theories for calculating spin-wave lifetimes, while Halperin and Hohenberg[19] attacked the problem from a macroscopic hydrodynamic point of view. All came to the same basic conclusion, namely that spin-wave linewidths should vary essentially as the fourth power of q within the hydrodynamic regime.

Since the energies of small-q spin waves are proportional to the square of q, it is evident that values of q can always be found small enough such that the energies of the excitations will be large compared to their widths. Thus, hydrodynamic spin waves can be expected to exist as well-defined excitations arbitrarily close to T_C, and it will be convenient to have methods of computing their energies. Unfortunately, although Dyson-Maleev theory converges rapidly when $C(T)/S < \frac{1}{3}$, i.e., $T < 0.8T_C$, it fails to converge at higher temperatures. Near T_C, however, spin-wave renormalization can be approached from a different point of view. According to the dynamic scaling arguments of Halperin and Hohenberg, the spin-wave stiffness constant in the hydrodynamic regime close to T_C should vary as the $\nu' - \beta$ power of the reduced temperature $|T - T_C|/T_C$. Joining Dyson-Maleev theory to a power law with exponent $\nu' - \beta = 0.69 - 0.36 = 0.33$ thus provides a method of predicting small-q spin-wave energies at essentially any temperature below T_C. As will be shown in Sec. V, this combination of methods is extremely effective for EuO.

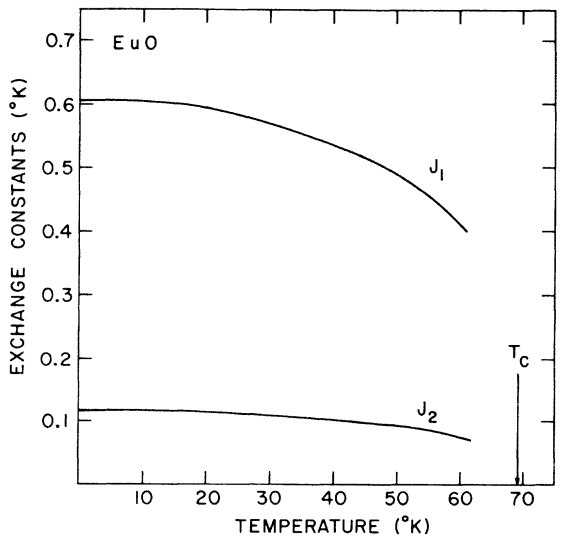

FIG. 1. Calculated renormalization of the nearest- and next-nearest-neighbor exchange constants of EuO using Dyson-Maleev theory including the effects of dynamical but not kinematical interactions.

Returning to the question of spin-wave lifetimes, let us briefly outline the predictions of the most recent theories. Considering first the work of Vaks *et al.*,[13] they looked in detail at two contributions to spin-wave damping, one associated with interactions between transverse fluctuations, i.e., spin-wave–spin-wave scattering, and the other with interactions between transverse and longitudinal fluctuations. Of these the former turned out to be the more important within the temperature and wave-vector range of our measurements.

In the hydrodynamic regime near T_C Vaks *et al.* found the spin-wave–spin-wave damping to be of the form

$$\Gamma_{t-t} \propto (1 - T/T_C)^{-2} \tilde{q}^4 [\ln(2/\tilde{q}^2)]^2 , \qquad (4a)$$

where $\tilde{q}^2$ represents the dimensionless quantity $\frac{1}{3}[\sum_r r^2 J(r)/\sum_r J(r)]q^2$, which has the value $4.8q^2$ for EuO when q is expressed in Å^{-1}. Harris[29] obtained an expression for the spin-wave damping with approximately the same q dependence as Eq. (4a) in the region accessible to neutron measurements.

The damping coefficient Γ_{t-t} has also been calculated by Halperin and Hohenberg using a combination of macroscopic-spin-wave[30] and dynamical scaling theory.[19] This led them to predict that Γ_{t-t} should vary as q^4 and as the $-\frac{3}{2}\nu'$ power of the reduced temperature, ν' being the exponent describing the divergence of κ_1 near but below T_C. Assuming $\nu' = \nu = 0.69$ (see Table IV of paper II), it then follows according to Halperin and Hohenberg that

$$\Gamma_{t-t} \propto (|T - T_C|/T_c)^{-1.04} q^4 . \qquad (4b)$$

The two equations predict nearly the same wave-vector dependence when $\tilde{q} \lesssim 0.01$, but for larger q their temperature and q dependence is quite different. In fact when $\tilde{q} \sim 0.4$, Eq. (4a) predicts not a fourth-power variation with q but something more like a power law with exponent 2.4. Concerning the q dependence, Halperin and Hohenberg themselves expressed reservations about the use

of macroscopic-spin-wave theory in this application. On the other hand, with regard to temperature dependence, it should be noted that Vaks *et al.* used self-consistent-field theory which gave mean-field exponents for static quantities and it would, therefore, hardly be surprising if their approach also failed to predict correctly the temperature dependence of dynamic quantities near T_C. Faced with a choice, we are inclined to take from each theory those results which appear to be best founded, namely, Vaks *et al.*'s prediction of the q dependence of the spin-wave damping coefficient and Halperin and Hohenberg's prediction of how it should vary with $(T - T_C)/T_C$.

Thus we come to view the transverse part of $F(q, \omega)$ as a function with two peaks centered at energies $\pm\hbar\omega_{\vec{q}}(T)$ representing propagating spin-wave modes. The exact analytical form is not specified by any of the existing theories. To calculate excitation energies we use either Dyson-Maleev theory [Eqs. (1)–(3)] or, at high temperatures and small values of q, the dynamical scaling relation $D(T) \propto (|T - T_C|/T_C)^{\nu'-\beta}$.

At low temperatures, spin-wave linewidths are expected to be too small to be detectable with the techniques currently available. Near T_C, however, spin-wave damping should be experimentally observable. In this regime we expect that the damping coefficient will vary with q as $\tilde{q}^4[\ln(2/\tilde{q}^2)]^2$ and with T as $(|T - T_C|/T_C)^{-1.04}$.

2. *Longitudinal spin fluctuations*

As far as we can determine, the only presently available treatment of longitudinal spin fluctuations in the ferromagnet below T_C is that of Vaks *et al.*[13] In their analysis they considered two relaxation mechanisms, spin diffusion and the coupling of longitudinal with transverse fluctuations. For spin diffusion they found the static susceptibility to be of the Ornstein-Zernike form $(q^2 + \kappa_1^2)^{-1}$ and the spectral weight function to be a single Lorentzian peak centered at zero energy. The second process involving the interaction of longitudinal fluctuations with spin waves is probably the more important in the isotropic ferromagnet at small values of q and ω because of the high density of small-q spin waves. For this mechanism they obtained a static susceptibility which varied inversely with q and a spectral weight function of the form

$$\frac{1}{\omega}\ln\left(\frac{1-\exp[-(\hbar\omega+\hbar\omega_{\vec{q}})^2/4\hbar\omega_{\vec{q}}\,kT]}{1-\exp[-(\hbar\omega-\hbar\omega_{\vec{q}})^2/4\hbar\omega_{\vec{q}}\,kT]}\right), \tag{5}$$

a function with two broad peaks centered at the spin-wave frequencies $\pm\hbar\omega_{\vec{q}}$. Thus, for a ferromagnet Vaks *et al.* lead us to expect the longitudinal part of $F(q, \omega)$ to consist of a small central peak associated with spin diffusion and a pair of much larger peaks at the spin-wave frequencies owing to the coupling of longitudinal fluctuations with the spin-wave modes.

B. $T > T_C$: Hydrodynamic regime

More than 20 years ago, Van Hove[31] suggested that the magnetization density $M(\vec{r}, t)$ in a paramagnet obeys a diffusion equation of the form $\partial M/\partial t = \Lambda_T \nabla^2 M$, and showed that in the limit of vanishing q and ω this led to a spectral weight function of the form

$$F(q, \omega) \to \frac{1}{\pi}\frac{\Lambda_T q^2}{(\hbar\omega)^2 + (\Lambda_T q^2)^2}. \tag{6}$$

Somewhat later de Gennes[15] calculated the second and fourth moments of the spectral weight function for a simple cubic magnetic lattice with nearest-neighbor couplings and found that both $\langle\omega^2\rangle$ and $\langle\omega^4\rangle$ had finite values and were proportional to q^2 in the small-q limit. Thus it was evident that Van Hove's Lorentzian form, which has infinite second and fourth moments, puts too much of the spectral weight at large values of ω. To remedy this, de Gennes suggested a truncated Lorentzian

$$F(q, \omega) = \begin{cases} \dfrac{1}{\pi}\dfrac{\Lambda_T q^2}{(\hbar\omega)^2 + (\Lambda_T q^2)^2}, & |\omega| < \omega_c \\ 0, & |\omega| > \omega_c \end{cases} \tag{7}$$

which has the convenient property that the diffusion coefficient Λ_T and cutoff frequency ω_c are related to $\langle\omega^2\rangle$ and $\langle\omega^4\rangle$ by the simple expressions

$$\Lambda_T q^2 = (\pi/2\sqrt{3})(\langle\hbar\omega^2\rangle^3/\langle\hbar\omega^4\rangle)^{1/2} \tag{8a}$$

and

$$\omega_c^2 = 3\langle\omega^4\rangle/\langle\omega^2\rangle. \tag{8b}$$

Thus the problem of calculating Λ_T reduces to one of determining $\langle\omega^2\rangle$ and $\langle\omega^4\rangle$. Alternatively, Mori and Kawasaki[16] and Bennett and Martin[17] chose to express Λ_T as a Gaussian function of ω rather than arbitrarily truncating the Lorentzian distribution at a particular frequency ω_c. As a consequence of their differing approaches, the diffusion coefficient as defined by de Gennes is smaller by a factor of $(6/\pi)^{1/2}$ than that defined by Bennett and Martin.

Collins and Marshall[32] have given prescriptions for calculating the moments of Heisenberg systems in the high-temperature limit and used them to obtain general expressions for both $\langle\omega^2\rangle$ and $\langle\omega^4\rangle$. Applied specifically to simple cubic lattices with nearest-neighbor interactions, their expressions reduce to those earlier derived by de Gennes. When substituted into Eq. (8a), Collins and Mar-

shall's formulas yield for cubic polycrystals with nearest-neighbor interactions the expression

$$\Lambda_\infty = \frac{\pi J a^2}{3}\left(\frac{S(S+1)}{z-1-3/[8S(S+1)]}\right)^{1/2} \tag{9}$$

(details of the derivation of this expression are given in Ref. 26, p. 496). For EuO, $S=\frac{7}{2}$, $J \approx J_1 + J_2 = 0.063$ meV, $a = 5.14$ Å, and $z = 12$. Inserting these values into Eq. (9) and multiplying the result by $(6/\pi)^{1/2}$ we obtain $\Lambda_\infty = 2.9$ meV Å^2.

To gain some insight into the temperature variation of Λ_T, we turn to the work of Bennett and Martin[17] and of Kawasaki.[33] Near T_C both find that

$$\Lambda_T = 0.15 z^{3/4}[S(S+1)]^{1/2} J a^2 (v/a^3)^{1/2}[\chi_{q=0}(T)/\chi_0]^{-1/4}, \tag{10}$$

where v represents the unit-cell volume and the other quantities have either been defined above or in Sec. II of paper II.[34] Dynamical scaling arguments suggesting that the diffusion constant should vary as the $-\frac{1}{4}$ power of the reduced susceptibility also support this relation. The coefficient of $[\chi_{q=0}(T)/\chi_0]^{-1/4}$ in Eq. (10) has the value 3.2 meV Å^2 for EuO. Using the customary power law $\chi_{q=0}(T)/\chi_0 = C(1 - T_C/T)^{-\gamma}$ to describe the temperature dependence of the reduced susceptibility together with Ritchie and Fisher's[35] series-expansion values $C = 0.87$ and $\gamma = 1.375$, we obtain as the best current estimate of the diffusion constant of EuO near T_C:

$$\Lambda_T = 3.3(1 - T_C/T)^{0.34}, \tag{11}$$

expressed in units of meV Å^2.

Thus theory leads us to expect a Lorentzian spectral weight function like that of Eq. (6) in the hydrodynamic regime above T_C. The spin diffusion constant, given near T_C by Eq. (11), is predicted by Eq. (9) to approach a limiting value of about 2.9 meV Å^2 at high temperatures. It should be emphasized that these equations apply only when $q \ll \kappa_1$. Within this limit, however, the half width of $F(q, \omega)$ is expected to vary quadratically with q (kinematical slowing down) and as the 0.34 power of the reduced temperature (thermodynamic slowing down) in the paramagnetic regime near T_C.

C. Critical regime

Earlier, we remarked that existing theory can tell us little about dynamical behavior in the critical regime below T_C. At and above T_C, however, the theory is sufficiently well developed to provide a qualitative and even, to some degree, a quantitative picture of critical spin dynamics. There are two basic approaches which will be of interest to us here; dynamical scaling as embodied in the work of Halperin and Hohenberg[19] and mode-mode coupling theories associated with the names of Kawasaki,[33,36] Wegner,[37] de Leener and Résibois,[38] Blume and Hubbard,[39] Hubbard,[23] Reiter,[40] and Månson and Sjöllander.[18]

Considering first the dynamical scaling approach, we already noted that at the ordering temperature it tells us that the characteristic frequency of the spectral weight function should vary as $q^{5/2}$ for ferromagnets. This is evident from the basic scaling equation $\hat{\omega}_q(\kappa_1) = q^{5/2}\Omega(\kappa_1/q)$ since $\Omega(\kappa_1/q)$ becomes independent of q in the limit $\kappa_1 \to 0$. We also mentioned Résibois and Piette's calculation of the normalized scaling function $\Omega(\kappa_1/q)/\Omega(0)$ and remarked that this permits the scaling equation to be used to predict the variation of the characteristic frequency of $F(q, \omega)$ everywhere above T_C. But Résibois and Piette's theory, although a considerable step forward, still leaves undefined the actual form of the spectral weight function. To determine $F(q, \omega)$ we must turn to the microscopic theories.

It is usual to approach microscopic spin dynamics through the Fourier transform of $F(q, \omega)$, the so-called relaxation function $f(q, t)$ which represents in this case the time decay of the magnetization following the switching off at time $t = 0$ of a spatially periodic magnetic field with wave vector $\vec{q}$. It is convenient to express the time derivative of $f(q, t)$ in terms of Mori's generalized Langevin equation[41]

$$\frac{\partial f(q,t)}{\partial t} = -\int_0^t k(q, t-t') f(q, t')\, dt', \tag{12}$$

where the quantity $k(q, t)$ is the memory function which relates $\partial f(q, t)/\partial t$ at a particular time t to a weighted sum over its values at earlier times. The central problem in the theory is thus to obtain a realistic representation of $k(q, t)$.

Of the methods for doing this, the one of most direct interest to us in terms of our investigations of EuO is that of Hubbard.[23] Using the equations of motion of a system of exchange-coupled spins, Hubbard derived for $k(q, t)$ an expression of the form

$$k(q,t) = \frac{2k_B T}{\chi_q}\sum_{q'}(J_{q'} - J_{q-q'})\chi_{q'} f(q', t) f(q-q', t) \tag{13}$$

where $J_q = \sum_j J_{ij}\exp(i\vec{q}\cdot\vec{r}_{ij})$. When Eq. (13) is substituted into Eq. (12) an integro-differential equation for $f(q, t)$ results. This Hubbard solved numerically for the special case of a simple cubic ferromagnet with only nearest-neighbor exchange. The spectral weight functions were then obtained by Fourier transforming the solutions.

Hubbard also investigated a number of general properties of his formalism. First, he found that it leads to the expected diffusive behavior in the limit of small q and that the diffusion coefficient

Λ_T calculated from the theory in the high-temperature limit agrees well with that obtained by other methods. Second, he showed that in the critical regime near T_C the diffusion coefficient is predicted by the theory to be proportional to $[\chi_{q=0}(T)/\chi_0]^{-1/4}$, consistent with dynamical scaling. Finally, for small values of q Hubbard showed that the spectral weight functions are of the form required by dynamical scaling, i.e., $F(q,\omega) \propto \hat{f}(\hbar\omega/\sigma q^{5/2}, \kappa_1/q)$, where

$$\sigma^2 = \frac{v(\sum_j |\vec{r}_{ij}|^2 J_{ij}) k_B T_C}{24\pi^3} \frac{T}{T_C}, \tag{14}$$

with v being the volume of the unit cell. The quantity σ depends on the strength of the exchange and on the lattice structure and is only weakly temperature dependent. On the other hand, $\hat{f}$ is to be regarded as a universal function in the sense that it is independent of crystallographic direction, lattice structure, spin, and the strength and range of interaction (provided the interaction is not truly long ranged). From the form of $F(q,\omega)$ it follows that the characteristic frequency will have the temperature and q dependence required by dynamical scaling. Thus Hubbard's theory is consistent with all presently known limiting conditions on dynamical behavior.

The half width of $F(q,\omega)$ is given by Hubbard in terms of a relation of the form

$$\hbar\Gamma(q,T) = \sigma q^{5/2} \mathcal{G}(\kappa_1/q), \tag{15}$$

where $\mathcal{G}(\kappa_1/q)$ is a function with the same qualitative behavior as the scaling function of Résibois and Piette[22] exhibiting a broad shallow minimum near $\kappa_1/q = 1$. Hubbard's computations do not accurately determine $\mathcal{G}(\kappa_1/q)$ in the limit $\kappa_1 \to 0$, i.e., when $T \to T_C$, but he estimates its value to be between 4.1 and 4.5. For EuO, $\sigma = 1.64$ meV Å$^{5/2}$ at T_C. Thus according to Eq. (15) the half width of the spectral shape function of EuO at T_C should be

$$\hbar\Gamma(q,T_C) \approx 7q^{5/2} \text{ meV} \tag{16}$$

when q is expressed in Å^{-1}.

It is of interest to compare this prediction with one made at about the same time by Riedel.[42] On the basis of the mode-mode approximation he obtained an expression for the linewidth of the isotropic ferromagnet at T_C of the form

$$\hbar\Gamma(q,T_C) = 4.10 Q q^{5/2}, \tag{17}$$

where (in our notation) the quantity

$$Q^2 = v k_B T_C (\mu_B g)^2 r_1^2 / 8\pi^3 \chi_0,$$

r_1 being the correlation strength defined by the relation $\chi_{q=0}/\chi_0 = (r_1\kappa_1)^2$. For EuO, $Q = 1.56$ meV Å$^{5/2}$. Equation (17) therefore leads to the prediction

$$\hbar\Gamma(q,T_C) = 6.4 q^{5/2} \text{ meV}, \tag{18}$$

in quite reasonable agreement with Hubbard's estimate.

The spectral weight functions Hubbard computed for the simple cubic ferromagnet with nearest-neighbor interactions are very nearly Lorentzian when $\kappa_1/q \gtrsim 1$ except at T_C where the shape becomes somewhat squarer. At temperatures above T_C and for values of $\kappa_1/q < 1$, the spectral weight functions also tend to be squarer than the Lorentzian form. Ultimately, at the largest values of q they evolve into a shape with a peak at finite frequencies reminiscent of damped propagating modes.

Before concluding this discussion of Hubbard's theory, it might be well to also take note of its more important limitations, especially with respect to application to EuO, First, there is the question of whether calculations for a simple cubic lattice with only nearest-neighbor interactions are applicable to EuO which has a fcc magnetic lattice and significant next-nearest-neighbor exchange. Second, and probably more important, Hubbard assumes that nearest-neighbor spins are not strongly correlated. While undoubtedly acceptable at high temperatures, this approximation is almost surely unrealistic at lower temperatures and raises questions about the reliability of the line shapes calculated near T_C. Finally, Hubbard considers spin couplings to arise purely from exchange mechanisms, ignoring dipolar interactions which are known to be important in EuO.

III. INSTRUMENTATION

All of the measurements to be discussed were made with a triple-axis spectrometer operated in the constant-q mode. Fixed neutron energies of either 4.8 or 13.5 meV were employed, depending on whether energy resolution or intensity was more important experimentally. Higher-order contamination was removed from the 4.8-meV beam by mounting in it a liquid-nitrogen-cooled polycrystalline beryllium filter; for the 13.5-meV beam a pyrolytic graphite filter was used.

With 4.8-meV incident neutrons, horizontal collimation was 40′ in front of the monochromating crystal, 20′ between the monochromating crystal and sample, 40′ between the sample and analyzing crystal, and 40′ between the analyzing crystal and detector. With 13.5 meV the corresponding collimations were either 20, 35, 35, 35, or 20, 35, 40, 25 depending on the circumstances. Both monochromating and analyzing crystals were pyrolytic graphite and had mosaic spreads of about 25′.

Details of sample preparation and sample char-

acteristics, thermometry, etc., are given in paper I, Sec. III C, and will not be repeated here.

IV. DATA ANALYSIS

A. Background corrections

In paper II we discussed at great length the sources of background in two-axis neutron scattering measurements. Here, we will be involved with three-axis spectroscopy and we can anticipate that background problems will be somewhat less severe because energy analysis will allow us to separate the elastic from the inelastic part of the scattering. Also, we can expect to be able to take advantage of the fact that some scattering mechanisms are temperature dependent. This, as will soon be evident, is very helpful in identifying and separating the various sources of background.

In general, in experiments of this type we can anticipate three major background contributions. These are (i) inelastic nuclear (phonon) scattering; (ii) room background; and (iii) elastic (incoherent) scattering from the sample and possibly from the sample cell, radiation shields, etc.

Phonon scattering will not be of concern to us here for the following reason: We can estimate the energy transfers involved in phonon scattering in EuO from the ultrasonic measurements of its elastic constants[43] and, according to these measurements, the sound velocity is never smaller than 2560 m/sec. This means that the initial slope of the phonon dispersion curve of EuO is never less than 16.8 meV/Å^{-1}. All of our measurements were made with considerably smaller energy transfers than 16.8 meV/Å^{-1} and thus were not within the range where single-phonon scattering could be observed. The same argument also applies to phonon scattering from the sample cell and radiation shields.

Room background is not expected to be energy dependent since it comes from neutrons which reach the detector without being reflected by the analyzer. Of course, the scattering from the room can, and often does, change in intensity as the position of the detector changes during an energy scan. To estimate room background we used two independent methods. First, by measuring the counting rate with the neutron beam stopped by a cadmium shutter mounted in front of the analyzer and, second, by determining the intensity in the far wings of the observed energy spectra. Both led to the same basic conclusion, namely, that the intensity of this part of the background was constant over the energy transfer range under investigation.

The third source of background, elastic incoherent scattering, is of greatest concern to us here because one of our major interests in this experiment is the study of magnetic line shapes near T_C where both transverse and longitudinal spectral weight function can be expected to center around zero energy transfer. Thus, if we wish to identify properly the magnetic contribution to the quasielastic scattering it will be essential to know, under given conditions, just how much of the observed intensity comes from elastic incoherent background.

Elastic incoherent scattering appears in our scans as a peak centered at zero energy transfer with a width characteristic of the spectrometer. This width is easily determined by replacing the sample with vanadium which is a purely incoherent scatterer. Since we are dealing with incoherent scattering of nuclear origin, we can expect the temperature and wave-vector dependence of this scattering to be solely determined by Debye-Waller factors which are essentially constant over the wave-vector and temperature range of interest. Hence this source of background should be independent of both temperature and wave vector while the magnetic scattering with which we are concerned will depend strongly on both quantities. For example, at low temperatures the inelastic magnetic scattering originates from the excitation of spin waves and, at finite values of the wave vector $\vec{q}$, spin-wave scattering will be associated with finite energy transfers. Therefore, the incoherent scattering (occurring at zero energy transfer) will not be contaminated by magnetic scattering. At temperatures above T_C, however, the magnetic scattering also centers at zero energy transfer but, at large values of q it spreads over so wide a range that the incoherent scattering is still distinguishable as a well-defined elastic peak on top of the broad magnetic line.

All of this is illustrated in Fig. 2, which shows

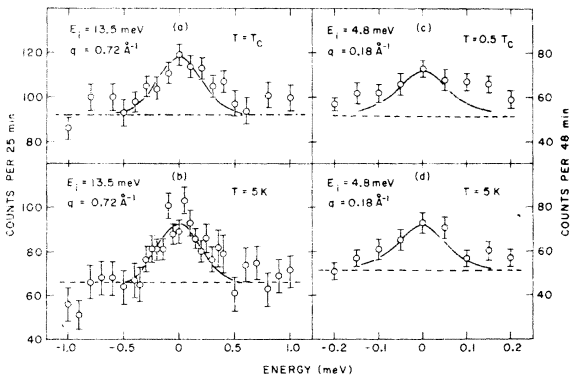

FIG. 2. Incoherent elastic background as observed at various temperatures, incident energies and wave vectors.

examples of the incoherent peak as observed under various conditions. The measurements labeled (a) and (b) were made with an incident neutron energy of 13.5 meV and with $q = 0.72$ Å^{-1}, while (c) and (d) were made with $E_i = 4.8$ meV and $q = 0.18$ Å^{-1}. The dashed lines indicate the intensities observed when the neutron beam was stopped with a cadmium shutter in front of the analyzer; the solid lines represent Gaussians with widths determined by the vanadium scans referred to earlier. At the low temperature (5 K) at which the (b) and (d) scans were made, the incoherent scattering appears as a well-separated peak. Curve (c) shows measurements made at $0.5T_C$ under experimental conditions otherwise identical to those of (d). As might be expected, the incoherent peak is not as well resolved at the higher temperature. This is due to scattering from slightly renormalized spin waves (in this case at about 0.4 meV) which is intense enough at the higher temperature to spill over into the neighborhood of the incoherent peak. Curve (a) shows results at T_C. These should be compared with (b) which was measured under the same conditions as (a) but at a temperature of 5 K. Obviously, the intensity is unchanged but at T_C the incoherent peak appears to be sitting on a broad, flat background. This is actually the magnetic scattering which (at the large value of q at which the measurements were made) is spread over a wide range of energy transfers.

B. Influence of dipolar interactions

We have already considered in Sec. IV of paper I how the spin-wave energies at low temperatures are influenced by dipolar interactions. There we noted that in general the effect of dipolar couplings is to increase the excitation energies except for modes propagating along the direction of spontaneous magnetization (the ⟨111⟩ direction in EuO) which are not influenced by dipolar forces. According to Eq. (5) of paper I, spin-wave energies are determined by an expression of the form

$$\hbar\omega(\vec{q}) = E_{ex}(\vec{q})[1 + \phi(\vec{q})\sin\theta_{\vec{q}}]^{1/2}, \qquad (19)$$

where $E_{ex}(\vec{q})$ represents the exchange part of the spin-wave energy, $\theta_{\vec{q}}$ is the angle between $\vec{q}$ and the direction of magnetization $\vec{M}$, and

$$\phi(\vec{q}) = 4\pi g\mu_B M/E_{ex}(\vec{q}).$$

Equation (19) includes both exchange and dipolar forces but assumes that no external magnetic field is present. In principle, if both M and $E_{ex}(\vec{q})$ are known, it is an easy matter to calculate the influence of dipolar interactions. In practice, however, the fact that we are concerned with measurements made on powder samples introduces computational complexities. These can be most easily understood by referring to Fig. 3. There, in (a) we show the line shape which would be expected at $q = 0.2$ Å^{-1} in a powder sample of EuO at low temperatures if it is assumed that exchange interactions alone are responsible for the magnetic couplings. As is evident, exchange interactions do not produce any significant anisotropy in the spin-wave energies at this small value of q. What would actually be observed with neutrons, however, would not be the sharp line of (a) but one which was "powder broadened" by the anisotropy of the spin-wave energies, the broadening arising in this case from dipolar rather than exchange interactions. Section (b) of the figure illustrates the effect of dipolar anisotropy on the powder-averaged spectrum. The line shape shown was obtained by calculating the spin-wave energies from Eq. (19) over a net of surface elements on a sphere of radius $q = 0.2$ Å^{-1} and grouping the energies into a ten-box density-of-states histogram. Both the broadening and the asymmetrical shape result from the variation of the factor $\sin^2\theta_{\vec{q}}$ in Eq. (19) with the direction of propagation. When this calculation is repeated for other values of q it is found that histograms like that of (b) are equally satisfactory representations of the orientationally averaged spectral distributions. As can be seen from Eq. (19), the relative width of the spectrum $E_{ex}(\vec{q})$ scales with q according to the relation

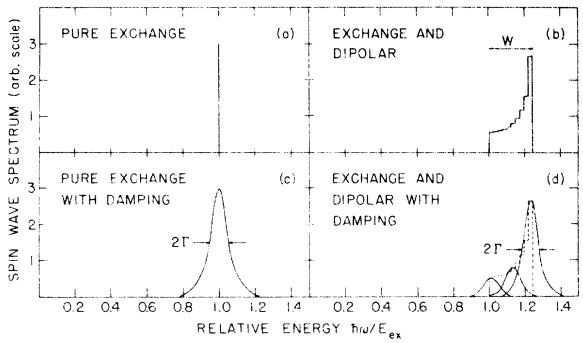

FIG. 3. Influence of dipolar interactions on the spin-wave line shape in a powder sample. (a) Sharp spin-wave line shape of a purely exchange-coupled idealized ferromagnet at small wave vectors and low temperatures. (b) Histogram representing the dipolar-broadened line shape. The width is typical of EuO at $q = 0.20$ Å^{-1}. (c) Line shape of small-q damped spin waves in a purely exchange-coupled ferromagnet. (d) Schematic representation of line shape when both dipolar broadening and damping are taken into account. The actual line shape in EuO at $q = 0.20$ Å^{-1} would be computed by replacing each box in the histogram in (b) by a bell-shaped curve like that of (c) but with identical area, not identical height as shown.

$$W/E_{ex}(\vec{q}) = \{E_{ex}(\vec{q})[1+\phi(\vec{q})]^{1/2} - E_{ex}(\vec{q})\}/E_{ex}(\vec{q})$$
$$= [1+\phi(\vec{q})]^{1/2} - 1, \quad (20)$$

with W being the full over-all width of the spectrum as shown in the figure.

Since in what follows we will only be concerned with small values of q, it will be sufficient for us to assume that dipolar anisotropy is the sole source of line broadening. It should be kept in mind, however, that exchange interactions play an increasingly important role at larger values of q and ultimately become the dominant broadening mechanism near the zone boundary.

What we have described thus far is the situation at low temperatures where the spin waves are well-defined excitations. At higher temperatures the excitations interact and broaden. The sharp-line spectrum of (a) accordingly acquires an intrinsic width 2Γ as shown in (c)—the damping coefficient Γ being, of course, one of the quantities of particular interest to us here. The appearance of an intrinsic width means that the orientational averaging will now involve a weighted sum of many broadened lines representing spin waves propagating in different crystallographic directions. We originally chose a histogram to represent the low-temperature spectral distributions rather than a continuous function because the higher-temperature distributions were then easily generated by simply replacing each box in the low-temperature histogram by a broadened curve of the same area with width 2Γ. Thus, for purposes of analysis the powder-broadened spectral distributions at finite temperatures (with dipolar interactions included) were represented as the sum of ten broadened curves distributed and weighted according to the low-temperature histograms but with an over-all width W which varies with temperature because it is dependent on both the magnetization and the renormalization of the exchange part of the spin-wave energies. Three of the ten broadened curves which together are intended to represent the spectral distribution observed in our neutron experiment are shown in (d).

C. Instrumental resolution

Like all observational instruments, the triple-axis neutron spectrometer is a device of limited resolution and as a consequence when it is set to observe a particular wave vector and energy transfer it actually samples a finite region of wave vector and energy space around the nominal setting. Our major interest is, of course, the dynamic structure factor $S(\vec{q}, \omega)$. To determine it accurately we have to unfold from the data the effects of instrument resolution. Normally this would be regarded as a straightforward procedure in triple-axis spectroscopy and would not be considered worthy of more than a passing comment. But our measurements were performed on a powder sample near the forward direction, i.e., around the 000 reciprocal-lattice point, and therefore differ to some extent from conventional triple-axis measurements. For this reason we will describe briefly the method used to unfold instrumental effects from the data.

Because of orientational averaging, the scattering function in a powder will depend only on the modulus of the wave vector $\vec{q}$ and the unfolding procedure (normally a four-dimensional unfolding involving q_x, q_y, q_z, and the energy transfer $\hbar\omega$) need therefore only be performed in two dimensions, i.e., $|\vec{q}|$ and $\hbar\omega$. It was consequently to our advantage in the long run to express the instrumental resolution function in terms of $|\vec{q}|$ and $\hbar\omega$ rather than the conventional four dimensions, although this did cause some initial complications because the four-dimensional resolution function can be treated as a product of four Gaussians while there is no equivalent simple analytic form in which the two-dimensional function can be cast.

To see why this is so consider the following: Assume that the spectrometer has been set at a nominal wave-vector transfer $\vec{q}$. Restricting our attention for the moment to the scattering plane, there are wave vectors both smaller and larger than $\vec{q}$ which contribute to the scattering and these, when transformed to $|\vec{q}|$ produce a symmetric distribution around $\vec{q}$. But because of finite vertical resolution, the distribution of wave vectors is shifted so that the average q is larger than the nominal q, or expressed in other words, the q distribution will always have greater weight on the large-q side of its nominal value.

To determine the "$|\vec{q}|$-resolution function," we divided the four-dimensional resolution ellipse into a fine grid and gave each subvolume $(\vec{q}, E)$ a specific resolution weight calculated using the Nielsen and Møller formalism.[44] Then the weight of each subvolume $(\vec{q}, \hbar\omega)$ was transferred to the appropriate subvolume $(|\vec{q}|, \hbar\omega)$ in the corresponding two-dimensional network. Separate two-dimensional networks were calculated for each measured point and stored in the computer for subsequent use in the unfolding process.

Unfolding was done by convoluting an assumed cross section containing adjustable parameters with the two-dimensional resolution function and then comparing the result with the measured intensity. A generalized linear least-squares method was used to find values of the cross-section parameters which minimized the weighted mean-square deviation between the calculated and mea-

sured intensities. Quality of fit was judged by calculating the quantity

$$\Delta^2 = \sum_i \frac{w_i[I_i(\text{meas}) - I_i(\text{calc})]^2}{N-n},$$

which, for a statistically satisfactory fit, should have a value of the order of unity. As is customary, the weight factor w_i in the above expression was assigned a value equal to the inverse of the square of the standard deviation of the measured intensity; N and n represent, respectively, the number of experimental points and the number of fitting parameters. Aside from an acceptable value of Δ^2, we also checked to see that the calculated intensities did not deviate systematically from the measured values.

V. EXPERIMENTAL RESULTS AND COMPARISONS WITH THEORY

A. Spin-wave renormalization and damping

Below T_C it is evident from the general form of Eq. (1) of paper II that the neutron cross section depends on how the scattering vector $\vec{\kappa}$ is oriented with respect to the direction of magnetization. Because our measurements were made on a multidomain powder near the forward direction where $\vec{\kappa} = \vec{q}$, what we will actually observe experimentally is the orientationally averaged cross section. In the notation of paper II, this can be written as

$$\frac{d^2\sigma}{d\Omega\, dE'} = A\frac{k_f}{k_i}\frac{\hbar\omega/k_BT}{1-\exp(-\hbar\omega/k_BT)} \times\chi_0^{-1}\left[\tfrac{2}{3}\chi_q^t F^t(q,\omega)+\tfrac{1}{3}\chi_q^l F^l(q,\omega)\right], \quad (21)$$

where the superscripts t and l refer, respectively, to the transverse and longitudinal response. [Details of the derivation of Eq. (21) can be found on pp. 242 and 243 of Ref. 26.) The coefficient A includes the magnetic form factor $\mathcal{F}(q)$ and a number of trivial constants. Since $\mathcal{F}(q)$ does not depart significantly from unity with the q range of our measurements, A is expected to be independent of both wave vector and temperature and is therefore treated as a normalization parameter when fitting Eq. (21) to experimental data.

χ_q^l and χ_q^t, the longitudinal and transverse parts of the static wave-vector-dependent susceptibility, were discussed in detail in paper II. This discussion suggests that below T_C the longitudinal part can be adequately represented by the expression

$$\frac{\chi_q^l}{\chi_0} \propto \frac{(T/T_C)^{\gamma'}}{[(a_{nn}\kappa_1)^2+(a_{nn}q)^2]^{1-\eta/2}}, \quad (22)$$

which is a simplified version of Eq. (5) of paper II indistinguishable experimentally from the original form. All of the parameters in Eq. (22) are known quantities for EuO. From paper II we have

$$T_C = 69.15 \text{ K},$$

$$\eta = 0.043,$$

$$a_{nn} = 3.63 \text{ Å},$$

$$a_{nn}\kappa_1 = F^-(1-T/T_C)^{\nu'} = 5.6(1-T/T_C)^{0.68},$$

and

$$\gamma' = \gamma = 1.39.$$

The value of η is the series-expansion estimate of Ritchie and Fisher.[35] To evaluate the last two quantities it was assumed that $\nu' = \nu$ and $\gamma' = \gamma$ as required by static scaling and consistent with the experimental observations discussed in Sec. VI of paper II.

For the transverse part of the static susceptibility below T_C we use the expression

$$\frac{\chi_q^t}{\chi_0} \propto \frac{T/T_C}{(a_{nn}q)^{2-\eta}}, \quad (23)$$

which is essentially Eq. (3) of paper II but modified so that χ_q^t becomes identical to χ_q^l in the limit $T \to T_C$. It may be arguable whether the q dependence of the transverse susceptibility is actually $q^{-2+\eta}$ rather than q^{-2}, but since η is a small quantity the difference is not important in practice. It should be noted that there are no adjustable parameters in either Eqs. (22) or (23)—all are either known from other experimental studies or are fixed by our two-axis measurements or theory.

The normalized spectral weight functions $F^l(q,\omega)$ and $F^t(q,\omega)$ are the objects of major interest in the present study. But as was remarked previously, it is necessary to assume analytic forms for these quantities in order to unfold instrumental resolution effects from the experimental data. In an earlier analysis[11] we tested three different analytical forms for $F^t(q,\omega)$; (i) a double Lorentzian, (ii) a damped harmonic oscillator, and (iii) an expression suggested by Halperin and Hohenberg.[19] All gave satisfactory fits to our experimental data when folded with the instrumental resolution but different values for the excitation energies and linewidths, particularly near T_C where the spin waves are heavily damped. While not in itself surprising, this difficulty does lend emphasis to a point which is often overlooked, namely, that near T_C it is not enough for a theory to predict spin-wave energies and linewidths—it must also specify the analytic form of $F^t(q,\omega)$ before precise comparisons with experiment can be meaningful.

In the majority of theories of spin dynamics below T_C a Lorentzian line shape is either explicitly or implicitly assumed for damped spin waves. We have therefore chosen to use a double-Lorentzian

form for the transverse spectral weight function in Eq. (21), i.e.,

$$F^t(q,\omega)=\frac{1}{2\pi}\left(\frac{\hbar\Gamma}{(\hbar\Gamma)^2+(\hbar\omega-\hbar\omega_q)^2}+\frac{\hbar\Gamma}{(\hbar\Gamma)^2+(\hbar\omega+\hbar\omega_q)^2}\right), \tag{24}$$

where $\hbar\omega_q$ defines the spin-wave energy and $\hbar\Gamma$ represents the linewidth [half-width at half-maximum (HWHM)]. In our fitting procedure both $\hbar\omega_q$ and $\hbar\Gamma$ were considered to be free parameters, or rather, to be more precise, the exchange part of the spin-wave energy, i.e., $E_{ex}(\vec{q})$ in Eq. (19), and $\hbar\Gamma$ were regarded as free parameters to be determined by fitting to the data.

Difficult as is the choice of the proper analytic form for $F^t(q,\omega)$, the question becomes even more perplexing for $F^l(q,\omega)$. It is evident from inspection of Fig. 6 of paper II that the longitudinal contribution to the magnetic scattering is only really observable within a narrow temperature range extending no more than four or five degrees below T_C, a temperature range within which the existing theory is probably not applicable. Ignoring this difficulty for the moment, we note that according to Vaks *et al.*,[13] $F^l(q,\omega)$ should contain a central peak associated with spin diffusion and a pair of side peaks at $\pm\hbar\omega_q$ due to the interaction of longitudinal with transverse spin fluctuations. We therefore attempted to fit our data to a three-peaked Lorentzian function—a central peak and a pair of side bands—but failed to obtain satisfactory fits in the neighborhood of zero energy transfer where the predicted line shapes always showed more intensity than was actually observed. Thus we were forced to conclude that the central peak, if it exists, is too small to be detectable in EuO with the techniques available to us and that the longitudinal part of the spectral weight function is of the same general functional form as the transverse part, namely, a pair of peaks centered at the spin-wave energies. At a later stage we will want to discuss this important conclusion further, but for the moment it will suffice simply to say that all of the line shapes we observed below T_C could be satisfactorily reproduced by assuming that both $F^t(q,\omega)$ and $F^l(q,\omega)$ had the double-Lorentzian form of Eq. (24). No doubt there are other two-peaked functions which would have fitted the data equally well, but the addition of a central peak of any significant weight does not appear to be acceptable from the experimental point of view.

A preliminary analysis of all of our measurements made not only below but also at and above T_C revealed that the best-fitting value of the normalization coefficient A in Eq. (21) was always close to 15.9. Therefore, in the final data reduction A was kept fixed at this value and only E_{ex} and $\hbar\Gamma$ were regarded as free parameters to be determined by fitting to the experimental observations.

Figure 4 shows typical line shapes observed below T_C. On the left-hand side of the figure are measurements made at various temperatures with q held fixed at 0.20 Å^{-1}; on the right-hand side are scans made at a constant temperature $(T_C - T)/T_C = 0.05$ with q varying. The measured intensities (corrected for background as described in Sec. IV A above) are indicated by the open circles while the solid lines represent the best least-square fits obtained by folding Eq. (21) with the instrumental resolution function. Equations (22) and (23) were used for χ_q^l and χ_q^t and Eq. (24) was taken to represent both $F^l(q,\omega)$ and $F^t(q,\omega)$. Table I gives the best-fitting values for E_{ex} and $\hbar\Gamma$ for all scans made below T_C. Note that the values of Δ^2 show no indications of systematic changes in the quality of the fits over the whole temperature range.

We will defer discussion of the spin-wave energies and linewidths to the following sections and only pause at this point to remark that the constancy of the normalization coefficient A is an indication that Eqs. (22) and (23) properly account for the temperature and wave-vector dependence of the static susceptibility. Furthermore, since at T_C one-third of the total intensity comes from longitudinal fluctuations, it is difficult to avoid

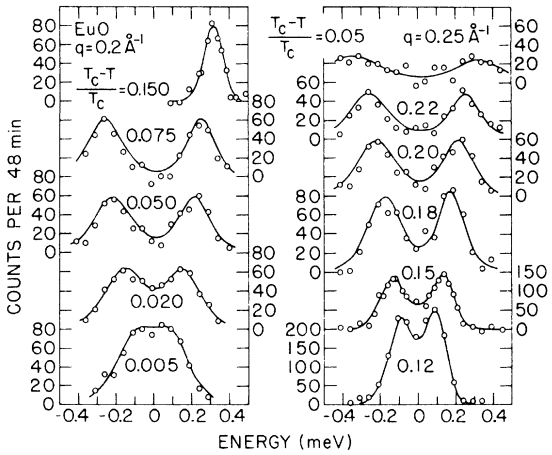

FIG. 4. Triple-axis scans below T_C in EuO. The points are the measured intensities with background subtracted while the lines represent the best fits to the data of a double-Lorentzian spectral weight function convoluted with the instrumental resolution. Note that no excess intensity is observed near zero energy transfer indicating that little, if any, spectral weight is associated with a central diffusive peak.

TABLE I. Exchange part of the spin-wave energies E_{ex} and line widths $\hbar\Gamma$ [half-width at half-maximum (HWHM)] for EuO as determined by the fitting procedure described in the text. Δ^2 indicates the weighted mean-square deviation as defined in Sec. IV C. Numbers in parentheses are the estimated uncertainties.

T(°K)	$(T_C - T)/T_C$	q(Å^{-1})	κ_1/q	Δ^2	$\hbar\Gamma$ (meV)	E_{ex} (meV)
10	0.855	0.20	···	0.79	0	0.43(1)
20	0.711	0.12	···	0.42	0	0.165(3)
20	0.711	0.15	···	0.81	0	0.238(6)
20	0.711	0.20	···	2.20	0	0.43(1)
30	0.566	0.09	···	2.79	0	0.075(4)
30	0.566	0.12	···	1.19	0	0.152(3)
30	0.566	0.15	···	0.83	0	0.230(4)
30	0.566	0.18	···	1.56	0	0.347(8)
30	0.566	0.20	···	0.75	0	0.423(6)
30	0.566	0.22	···	2.52	0	0.52(2)
58.79	0.150	0.20	2.11	1.48	0.020(5)	0.268(4)
62.25	0.100	0.09	3.55	2.73	0.013(3)	0.048(2)
62.25	0.100	0.12	2.66	3.87	0.020(4)	0.085(5)
62.25	0.100	0.15	2.13	2.46	0.022(5)	0.127(5)
62.25	0.100	0.18	1.78	1.11	0.027(5)	0.203(6)
62.25	0.100	0.18	1.78	1.94	0.033(6)	0.182(8)
63.98	0.075	0.20	1.31	1.32	0.046(5)	0.214(6)
65.71	0.050	0.12	1.66	0.98	0.020(3)	0.061(2)
65.71	0.050	0.15	1.33	1.94	0.027(3)	0.097(3)
65.71	0.050	0.18	1.11	1.64	0.045(5)	0.143(5)
65.71	0.050	0.20	1.00	1.60	0.057(6)	0.182(6)
65.71	0.050	0.22	0.91	1.84	0.060(7)	0.221(8)
65.71	0.050	0.25	0.80	1.11	0.10(2)	0.30(2)
67.10	0.030	0.20	0.70	0.97	0.058(5)	0.146(5)
67.79	0.020	0.20	0.54	0.50	0.070(4)	0.128(3)
68.48	0.010	0.20	0.33	1.76	0.063(8)	0.096(7)
68.82	0.005	0.20	0.21	0.61	0.063(5)	0.079(5)
68.82	0.005	0.25	0.17	1.51	0.17(3)	0.13(4)

concluding that the contribution of longitudinal fluctuations to the intensity slightly below T_C is contained within the double-Lorentzian function used to represent both $F^l(q,\omega)$ and $F^t(q,\omega)$. This appears to rule out the possibility that $F^l(q,\omega)$ is actually a very broad central peak indistinguishable from background on the scale of our measurements. For if this were in fact the case, the broad peak would at some point have had to narrow rapidly to match the observed linewidth at T_C and would therefore have produced a systematic change in the value of the normalization coefficient A in the vicinity of T_C. Nothing like this was observed.

All of the measurements discussed thus far involved spin waves with wave vectors less than 0.25 Å^{-1}. In Ref. 12 there are data for the same EuO sample for larger values of q. These have been listed in Table II as a convenience since they will be needed in Sec. V A 1 for analysis of spin-wave renormalization.

1. Renormalization of spin-wave energies

As was noted in Sec. II A, the large spin of the europium ion ($S=\frac{7}{2}$) means that a calculation of spin-wave renormalization based solely on the dynamical spin interaction, i.e., neglecting the effects of the kinematic interaction, should re-

TABLE II. Spin-wave energies and linewidths for EuO at large wave vectors from Ref. 12.

	Spin-wave energy (meV)			Linewidth (HWHM) (meV)		
T(°K)/q(Å^{-1})	0.60	0.80	1.00	0.60	0.80	1.00
20	3.20(2)	4.61(3)	5.51(5)	~0	~0	~0
40	2.83(2)	4.08(5)	4.97(7)	~0	0.14(7)	0.24(8)
50	2.56(5)	3.65(6)	4.48(8)	0.14(5)	0.23(8)	0.36(9)
60	1.99(7)	3.15(10)		0.4(1)	1.1(2)	

main valid to reasonably high temperatures. We find in fact that a self-consistent calculation of the renormalized exchange constants based on the procedure outlined in Sec. II A converges at all temperatures below 62 K ($0.9T_C$). Only above this temperature does the calculation fail.

To make a direct comparison of the predictions of Dyson-Maleev renormalization theory with experiments on a powder sample it is of course necessary to average the calculated spin-wave energies over all directions of propagation as explained in Sec. IV B. This was done by using the computed renormalized exchange constants plotted in Fig. 1. In making the computations, we included the dipolar contribution to the spin-wave energies as given by Eq. (19) and used the measured reduced magnetization as given in paper II (see in particular Fig. 11). The resulting directionally averaged energies are plotted as the solid lines in Fig. 5. Also shown are the experimentally observed spin-wave energies including measurements from paper I and those listed in Tables I and II. Agreement is strikingly good, the maximum difference between computed and observed values being 15% at $q = 0.2$ Å^{-1} and $T = 60$ K.

All of the measurements made near T_C involved wave vectors so small that the exchange part of the spin-wave energies could be satisfactorily represented by the simple expression $E_{ex}(q) = D(T)q^2$. Using the values of E_{ex} listed in Table I it is easy to derive the stiffness constant $D(T)$. The result, shown in Fig. 6, can be regarded as indicating how the exchange part of the magnetic interaction renormalizes since $D(T) = 2a^2S[J_1(T) + J_2(T)]$. Fitting the data in the region $0.005 \leq 1 - T/T_C \leq 0.15$ to a power law of the form

$$D(T)/D(T=0) = D^*(1 - T/T_C)^{\mu} ,$$

we find $D^* = 1.17 \pm 0.03$ and $\mu = 0.37 \pm 0.01$. This best-fitting power law appears as the dash-dotted line in the figure. The observed value of the exponent is slightly larger than the value $\mu = \nu' - \beta = 0.32 \pm 0.02$ predicted by dynamical scaling (assuming that $\nu' = \nu$ and using the values for ν and β listed in Table IV of paper II). For comparison the dashed line in the figure is plotted with slope 0.32 as predicted by theory. The fact that the dashed line lies above the measured values should be disregarded since it was arbitrarily joined to the calculated exchange renormalization curve at the point where the calculation ceased to converge. And, as we have already noted, the self-consistent calculation overestimates the exchange energies at small values of q and at temperatures near 60 K ($1 - T/T_C = 0.15$) by about 15%.

We do not consider the difference between the experimental value of μ and that predicted by dynamical scaling theory to be significant. The reason for this is that the values of $D(T)$ derived from the data become sensitive to the assumed form of $F^t(q, \omega)$ whenever there is appreciable overlap between the annihilation and creation peaks in the measured spectrum. This is true

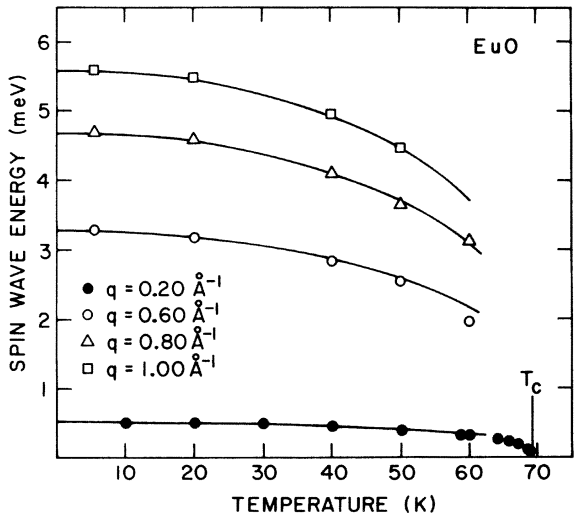

FIG. 5. Renormalization of spin-wave energies in EuO. The measurements at 5.5 K are taken from paper I, those at $q = 0.20$ Å^{-1} are from the present study, and the rest are reproduced from Ref. 12. The lines represent calculations based on Dyson-Maleev theory and include both the exchange and dipolar contributions to the spin-wave energies. For the calculations we used the renormalized exchange constants shown in Fig. 1 and the measured temperature variation of the magnetization shown in Fig. 11 of paper II.

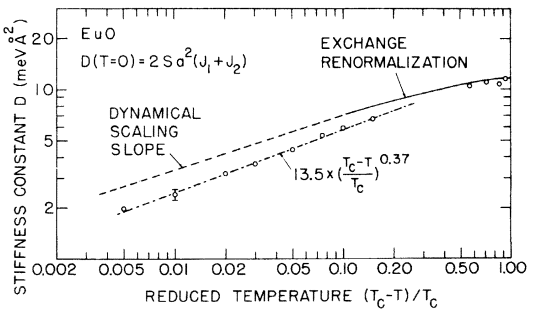

FIG. 6. Renormalization of the spin-wave stiffness constant $D(T) = E_{ex}q^2$. In the temperature region below 62 K, i.e., for $0.10 < (T_C - T)/T_C < 1$, the renormalization was calculated self-consistently including the dynamical spin-wave interaction. This is shown as the solid line. Near T_C, dynamical scaling predicts a power-law behavior $D(T) \propto [(T_C - T)/T_C]^{\nu' - \beta}$. The dashed line with slope $\nu' - \beta = 0.32$ is drawn as an extension of the calculated exchange renormalization curve. The dashed-dotted line is the best power-law fit to the measurements.

irrespective of whether the overlap is due to finite experimental resolution, to spin-wave damping or to a combination of both effects. If for example we had used the Halperin-Hohenberg form of $F^t(q,\omega)$ instead of the double Lorentzian of Eq. (24), we would have found $\mu = 0.33$ as was noted in Ref. 11. Discrepancies of the order of 15% in μ have therefore to be regarded as within the systematic error limits of the data analysis.

2. *Damping of spin waves*

Let us now turn to consideration of the temperature and q dependence of $\hbar\Gamma$, the spin-wave linewidth. The data in Table I cover the temperature range $0.15 \geq 1 - T/T_C \geq 0.005$ and wave vectors between 0.09 and 0.25 Å^{-1}. Also listed in the table are values of κ_1/q calculated from the static measurements described in paper II. This ratio is included because it indicates whether the excitation is in the hydrodynamic regime where $\kappa_1/q \gg 1$, the critical regime where $\kappa_1/q \ll 1$, or somewhere between the two extremes. Earlier we noted that the existing theories of spin wave damping are only expected to apply in the hydrodynamic regime. Inspection of Table I makes it evident that few if any of our measurements fully satisfy this requirement—an unfortunate consequence of the finite limits of our experimental resolution. Nevertheless, it is of interest to compare our observations with the predictions of hydrodynamic damping theory if for no other reason that to establish a lower limit on the values of κ_1/q defining hydrodynamic excitations.

In Sec. II A we noted that within the q range of our measurements spin-wave scattering by longitudinal fluctuations is presumed to be unimportant and spin-wave damping is expected to arise primarily from spin-wave–spin-wave scattering. The microscopic theory of Vaks *et al.* predicts a damping coefficient of the form of Eq. (4a). This suggests that the linewidth ought to be represented as

$$\hbar\Gamma = \xi_T \tilde{q}^4 [\ln(2/\tilde{q}^2)]^2 , \qquad (25)$$

where for EuO the dimensionless quantity $\tilde{q}^2 = 4.8q^2$ as noted earlier. In the limit of very small values of q, the $\tilde{q}^4$ factor in Eq. (25) will dominate the logarithmic factor and the linewidth will become proportional to q^4; in other words, the damping coefficient will then go over to the form of Eq. (4b) which is based on macroscopic spin-wave theory. At the other extreme when q is so large that $\tilde{q}$ approaches unity, Eq. (4a) ceases to apply and Eq. (25) becomes meaningless. In the q range of interest here (0.1–0.4 Å^{-1}) the logarithmic factor has a substantial influence and in all likelihood, if we are anywhere near the hydrodynamic regime it would only be within the range of Eq. (25), not the small-q limit of the macroscopic theory.

To investigate this possibility let us look at the sequence of measurements in Table I made at a temperature of 65.71 K, which are the most complete set available. The observed linewidths at various values of q are plotted in Fig. 7. Also plotted is a dashed line indicating the q^4 variation predicted by the macroscopic theory. As expected, the increase in $\hbar\Gamma$ is not as rapid as q^4. But the solid line representing Eq. (25) with $\xi_T = 0.28 \pm 0.01$ is an excellent fit to the data. It is therefore tempting to conclude that spin-wave–spin-wave scattering is indeed the dominant decay mechanism and is satisfactorily described by the Vaks *et al.* theory. The dash-dotted curve in the figure is the result of a recent calculation by Raghavan and Huber[45] using a mode-mode coupling theory and including both exchange and dipolar interactions. Considering that there are no adjustable parameters in their theory, agreement with the

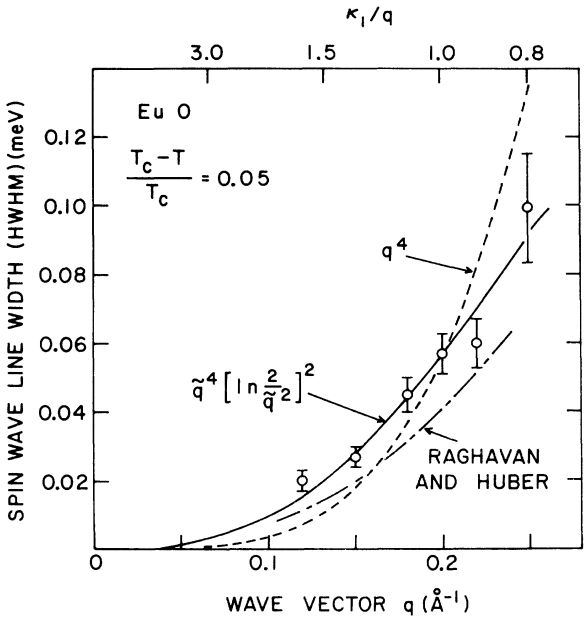

FIG. 7. q dependence of the spin-wave linewidths in EuO at $T = 65.71$ K. Macroscopic spin-wave theory predicts a linewidth proportional to q^4 in the small-q limit (dashed line). The logarithmic correction factor is introduced by microscopic theory. The solid line was normalized to give the best fit of the microscopic theory to the measurements; the dash-dotted line represents the prediction of Raghavan and Huber's mode-mode theory which includes dipolar as well as exchange interactions. From the κ_1/q scale at the top of the figure it is evident that the data are not entirely within the hydrodynamic regime.

experimental data is better than might reasonably be expected.

It is also of interest to investigate the temperature dependence of the spin-wave linewidths which we can do by using the measurements in Table I at values of q near 0.2 Å^{-1}. In the hydrodynamic regime, dynamical scaling predicts that the damping should be given by Eq. (4b), which means that the quantity ξ_T in Eq. (25) should be of the form

$$\xi_T = \xi_0(1 - T/T_C)^{3\nu'/2} , \tag{26}$$

where $\frac{3}{2}\nu' = 1.03$ for the Heisenberg ferromagnet (see Table IV of paper II). Alternatively, the theory of Vaks *et al.* predicts an exponent of 2 rather than 1.03.

Figure 8 shows the temperature dependence of the observed linewidths. Also included at the top of the figure, as a matter of interest, is an approximate κ_1/q scale. Equation (26) with $\frac{3}{2}\nu' = 1.03$ and $\xi_0 = 0.017$ meV is plotted as the solid line; the dash-dotted curve is the mode-mode calculation of Raghavan and Huber. Clearly, a temperature variation as rapid as that predicted by Vaks *et al.* is not acceptable. Dynamical

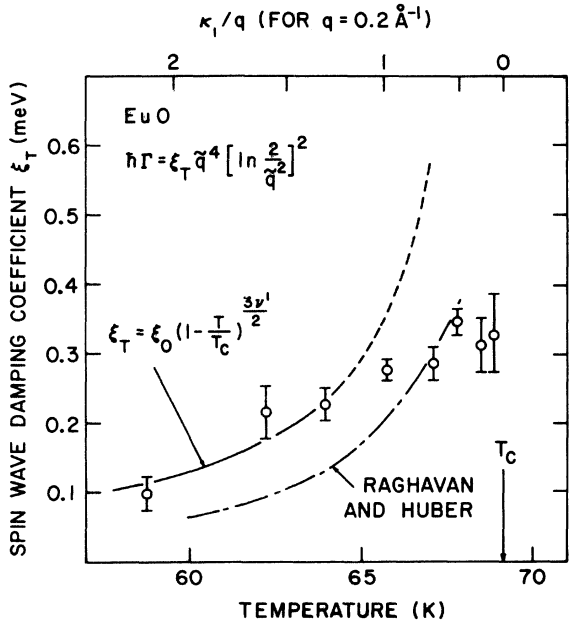

FIG. 8. Temperature dependence of the spin-wave damping coefficient ξ_T defined by Eq. (25) in the text. In the hydrodynamic regime $\kappa_1/q \gg 1$ dynamic scaling predicts the power-law behavior indicated by the solid line. The dash-dotted line represents the prediction of Raghavan and Huber's mode-mode theory which includes dipolar as well as exchange interactions. It is evident from the scale at the top that deviations from the hydrodynamic prediction develop at $\kappa_1/q \approx 1$.

scaling, as embodied by Eq. (26), does, however, provide a reasonable description of the data below 65 K, although at higher temperatures the linewidths break away from the power law and approach a limiting value of about 0.35 meV. This behavior could very well be indicative of the crossover from the hydrodynamic to the critical regime. According to the upper scale it takes place at $\kappa_1/q \approx 1$, consistent with the expectations of theory.

B. Spin diffusion above T_C

Having discussed collective spin motions below T_C let us now direct our attention to spin behavior above T_C, considering first spin fluctuations with wavelengths large compared to the size of the ordered magnetic clusters, i.e., fluctuations within the hydrodynamic regime for which $\kappa_1/q \gg 1$. For a number of reasons hydrodynamic theory above T_C is much simpler than its equivalent below T_C. First of all, the absence of long-range magnetic order means that the distinction between longitudinal and transverse fluctuations loses its meaning and we therefore need think only in terms of one type of fluctuation. Second, with no long-range order present hydrodynamic fluctuations diffuse but cannot propagate. As a consequence the spectral weight function becomes a single-peaked function centered at zero energy transfer and Eq. (21) describing the neutron scattering cross section reduces to the simpler form

$$\frac{d^2\sigma}{d\Gamma\, dE'} = A\frac{k_f}{k_i}\frac{\hbar\omega/k_BT}{1 - \exp(-\hbar\omega/k_BT)}\frac{\chi_q}{\chi_0}F(q,\omega) . \tag{27}$$

The reduced wave-vector-dependent susceptibility χ_q/χ_0 is expected to have the same form as Eq. (22) but $a_{nn}\kappa_1$ will be smaller by a factor of 2.4 above T_C as we noted in Sec. VI of paper II. For $F(q,\omega)$ we assume the Lorentzian form of Eq. (6), namely,

$$F(q,\omega) = \frac{1}{\pi}\frac{\hbar\Gamma}{(\hbar\Gamma)^2 + (\hbar\omega)^2} , \tag{28}$$

where the linewidth $\hbar\Gamma = \Lambda_T q^2$ as discussed in Sec. II B above.

When the data were analyzed with Eqs. (27) and (28), we found that the same normalization constant A applied equally well at all temperatures both above and below T_C. This not only indicates that Eq. (27) properly describes the temperature dependence of the scattered intensity but it also leaves only one parameter, the linewidth, to be determined by fitting the cross section to the individual scans.

Results of the analysis of measurements extending over the temperature range from T_C to

TABLE III. Linewidth $\hbar\Gamma$ and spin-diffusion coefficient Λ_T of EuO above T_C.

T(°K)	$(T-T_C)/T$	q(Å^{-1})	κ_1/q	Δ^2	$\hbar\Gamma$ (meV)	$\Lambda_T=\hbar\Gamma/q^2$ (meV Å^2)
71.38 [a]	0.031	0.18	0.34	1.09	0.055(3)	
75.19 [a]	0.080	0.18	0.67	0.77	0.045(3)	
76.20	0.093	0.09	1.50	0.56	0.011(1)	1.4(1)
76.20	0.093	0.12	1.12	1.32	0.025(3)	1.7(2)
76.20	0.093	0.15	0.90	1.29	0.042(3)	
83.10	0.168	0.18	1.19	1.38	0.063(6)	1.9(2)
85.36 [a]	0.190	0.18	1.32	0.92	0.067(6)	2.1(2)
91.71 [a]	0.246	0.15	1.98	0.55	0.035(6)	1.6(3)
98.36 [a]	0.297	0.12	2.96	2.15	0.027(8)	1.9(6)
98.36 [a]	0.297	0.18	1.97	1.26	0.073(11)	2.3(3)
113.60	0.391	0.12	3.94	0.46	0.030(2)	2.1(2)
113.60	0.391	0.15	3.15	0.76	0.051(4)	2.3(2)
113.60	0.391	0.18	2.63	0.63	0.091(6)	2.8(2)
121.39 [a]	0.430	0.12	4.40	0.60	0.028(5)	1.9(3)
130.20	0.469	0.12	4.89	6.67	0.034(6)	2.4(4)
130.20	0.469	0.15	3.91	1.45	0.060(5)	2.7(2)
130.20	0.469	0.18	3.26	1.39	0.11(1)	3.4(4)

[a] These measurements were made in sequence with those listed in Tables I and IV. See Sec. V B.

slightly less than $2T_C$ and over wave vectors from 0.09 to 0.18 Å^{-1} are given in Table III. Near T_C the region accessible to investigation was limited by our ability to resolve experimentally the intrinsic widths of the lines at small values of q while at high temperatures the fundamental limitation was the dwindling scattered intensity. Roughly half of the measurements listed were performed in sequence with measurements made at and below T_C. These are identified in the table. The comment made immediately above concerning the fixed value of A refers to these data. All of the other measurements were made with a different neutron spectrometer but using the same incident neutron energy. These were separately analyzed but also with a fixed value of the normalization constant for all scans.

As before, we tentatively assume that the measurements in Table III with values of $\kappa_1/q > 1$ fall within the hydrodynamic regime. Therefore, for these measurements we list in the last column in the table values of the diffusion constant $\Lambda_T = \hbar\Gamma/q^2$. These are plotted in Fig. 9 on a double log scale. It should be remarked that the large uncertainties and the scatter in the data reflect the fact that linewidths in EuO are almost two orders of magnitude smaller than those observed in ferromagnets such as iron[4] and cobalt[6] and are therefore difficult to measure accurately.

Also shown in Fig. 9 are the predictions of theory; namely, the temperature dependence of Λ_T near T_C, given by Eq. (12), and its limiting value at high temperatures as estimated from the moment calculations of Collins and Marshall.[32] Particular attention should be called to the fact that the comparison between experiment and theory is on an absolute scale and involves no adjustable parameters. Although the scatter in the data is larger than one might like, it nonetheless seems clear that the theory adequately describes the temperature variation of the spin diffusion constant and in addition predicts its magnitude with quite acceptable accuracy.

C. Critical region

1. Line shapes at T_C

In the immediately preceding sections, we have shown that the observed line shapes are well approximated by a pair of Lorentzian functions below T_C and by a single Lorentzian above T_C. Now let us focus our attention on the question of what hap-

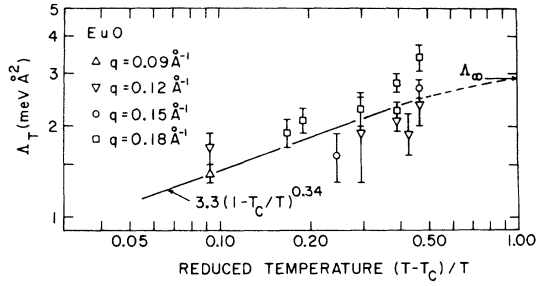

FIG. 9. Temperature variation of the spin-diffusion coefficient Λ_T of EuO within the hydrodynamic regime above T_C. The solid line represents the prediction of Bennett and Martin and of Kawasaki. Λ_∞ was obtained from Collins and Marshall's moment calculations.

pens to the line shape at T_C, the borderline between the two regions. As noted in Sec. II C, Hubbard's calculations suggest that at T_C the spectral weight function will have a somewhat squarer form reflecting the persistence of propagative-type spin motions within what has basically become a diffusive regime.

To look in detail at this problem, we fitted our data at T_C to two line shapes; the single Lorentzian of spin-diffusion theory and the squarer form suggested by Hubbard. Figure 10 shows the results for $q = 0.12$ and 0.42 Å^{-1}, the smallest and largest wave vectors investigated. One can see that the two line shapes are almost indistinguishable. Whatever differences there are appear most evident at $q = 0.42$ Å^{-1}. In this case the weighted mean-square deviation slightly favors the Hubbard form even though it seems to be flatter near the top of the peak than is indicated by the data.

Since we are unable to choose between the two line shapes experimentally and since we are also not sure that the Hubbard form is applicable to EuO (for the reasons outlined in Sec. II C), we decided to continue to use a Lorentzian spectral weight function to analyze the data at T_C. Not only

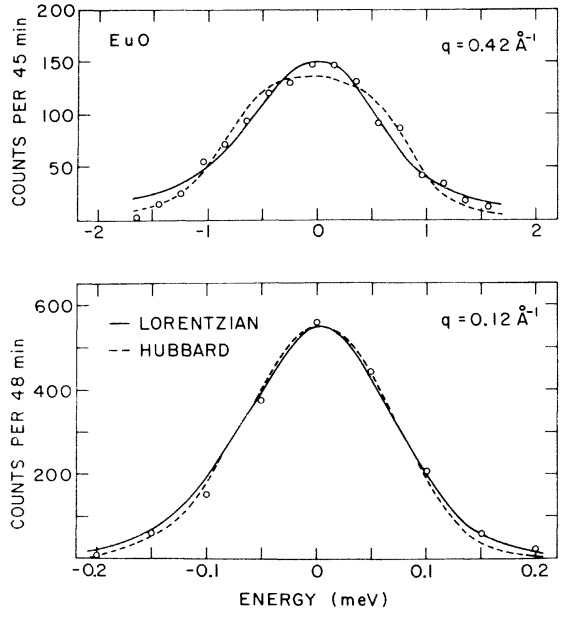

FIG. 10. Line shapes at T_C for the smallest and largest wave vectors investigated. The solid line is the best fit obtained by convoluting a Lorentzian spectral weight function with the instrumental resolution; the dashed line shows the effect of replacing the Lorentzian with Hubbard's spectral weight function calculated for a simple cubic ferromagnet with only nearest-neighbor interactions. Note the difference in the upper and lower energy scales.

is it more convenient to handle analytically, but there is the additional benefit that all of our linewidth analysis, from the lowest to the highest temperatures, is then based on spectral weight functions of a single form. This has the advantage of eliminating the possibility of systematic differences associated with changing from one functional form to another during the analysis.

2. *Linewidths at T_C*

Two separate series of measurements were made at T_C. For wave vectors less than 0.2 Å^{-1}, we used an incident neutron energy of 4.8 meV to optimize the experimental resolution. At larger values of q, however, we had to compromise on resolution by going to 13.5 meV to obtain satisfactory intensities. One can get an indication of the resolution change associated with the change in incident energy by referring to Fig. 2, which shows the observed energy widths of the incoherent elastic scattering.

As noted in Sec. V B, we used Eq. (27) to analyze the data at T_C with

$$\chi_q/\chi_0 = (a_{nn}q)^{-2+\eta} \tag{29}$$

as given by Eq. (22) and $F(q, \omega)$ of the Lorentzian form of Eq. (28). The normalization constant for the 4.8-meV scans was kept fixed at the same value used to analyze the scans above and below T_C. For the 13.5-meV scans the best over-all value of the normalization constant was first determined and it was then held fixed at that value for the final analysis. Thus only the linewidth $\hbar\Gamma(q, T_C)$ was determined by the final least-squares fitting. The results are listed in Table IV. Note that the values of Δ^2 are somewhat larger than those in Tables I and III indicating that the fits are not as good as those obtained above and below T_C. This may be evidence for the squarer spectral weight function suggested by Hubbard but, as we have said, the differences are not really significant at the level of precision of our measurements.

It is generally assumed that as a consequence of

TABLE IV. Linewidth of EuO at T_C.

q(Å^{-1})	$\hbar\Gamma_{T_C}$ (meV)	Δ^2
0.12	0.026(1)	1.1
0.15	0.047(3)	2.0
0.18	0.072(6)	2.7
0.20	0.095(10)	2.3
0.24	0.133(7)	4.6
0.30	0.22(1)	2.2
0.36	0.33(2)	2.5
0.42	0.48(3)	1.9

dynamical scaling the linewidth of an isotropic ferromagnetic will vary as $q^{5/2}$ at T_C, a relationship that has been observed to hold in both iron[3] and cobalt.[4] But when our measured values of $\hbar\Gamma(q, T_C)$ are plotted against $q^{5/2}$, as is done in the lower part of Fig. 11, it appears that the expected relationship is not actually observed over the whole q range investigated. Significant deviations occur at the smaller values of q. This is particularly evident when $\hbar\Gamma(q, T_C)/q^{5/2}$ is plotted against $q^{5/2}$, as is done in the upper part of the figure. The deviations call to mind the way the spin-wave energies depart from q^2 owing to dipolar influences and, as we will soon show, they are in fact related effects.

If we simply fit a power law to the linewidths observed at T_C we find that the expression

$$\hbar\Gamma(q, T_C) = (3.5 \pm 0.2)q^{2.29 \pm 0.03} \text{ meV} \tag{30}$$

is a good empirical representation of the data (q is here expressed in Å^{-1}). In fact, Eq. (30) fits the data so well that it is tempting to infer that dynamical scaling is not exactly obeyed in EuO. But we suggest that a more likely explanation is that dipolar interactions are responsible for the deviation. Our reasoning is as follows: The basis of the dynamical scaling hypothesis is the assumption that the characteristic frequency $\hat{\omega}_q(\kappa_1)$ is a homogeneous function of q and κ_1 and, as we earlier remarked, can be represented as

$$\hbar\hat{\omega}_q(\kappa_1) = q^u \Omega(\kappa_1/q) , \tag{31}$$

where $\Omega(\kappa_1/q)$ is the so-called scaling function and u is an exponent characteristic of the particular magnetic system. Equation (31) is expected to hold within the hydrodynamic regime at all temperatures. Below T_C, $\hbar\hat{\omega}_q(\kappa_1)$ becomes identical to the spin-wave energy Dq^2. Thus within the temperature range in which D is proportional to $\kappa_1^{1/2}$ we can write

$$\hbar\omega_q(\kappa_1) = Dq^2 = W\kappa_1^{1/2}q^2 = Wq^{5/2}(\kappa_1/q)^{1/2} = q^{5/2}\Omega(\kappa_1/q) , \tag{32}$$

where the constant $W = D^*D(T=0)(a_{nn}/F^-)^{1/2}$, F^- being the critical coefficient defined in Sec. VI of paper II and $D(T=0)$ and D^* the spin-wave stiffness constants defined in Sec. V A 1. At T_C, $\kappa_1/q = 0$ irrespective of the value of q and, consequently, the q dependence of $\hbar\hat{\omega}_q(\kappa_1)$—or, equivalently, the q dependence of the linewidth—comes from the $q^{5/2}$ factor alone. As it stands, however, this argument cannot be directly applied to EuO because even though D is proportional to $\kappa_1^{1/2}$, the spin-wave energy at small values of q is not proportional to Dq^2 because of dipolar interactions. To correctly describe the spin-wave energies we must use Eq. (6) of paper I, which tells us that the angularly averaged energies are given by the expression

$$\langle\hbar\omega(q)\rangle = Dq^2\left(\frac{1}{2} + \frac{1+\phi}{2\phi^{1/2}}\arctan\phi^{1/2}\right), \tag{33}$$

where the quantity $\phi = 4\pi g\mu_B M/Dq^2$ is independent of temperature because the magnetization M and the stiffness constant D have essentially the same temperature dependence. From the values of J_1 and J_2 given in paper I we fine $D(T=0) = 11.6$ meV Å^2. Using for the magnetization the value $4\pi M = 24$ KOe (from Ref. 8 of paper I) we find $\phi = 0.024q^{-2}$ when q is expressed in Å^{-1}. It is easy to see from a double log plot that over the wave-vector range of interest Eq. (33) is well fitted by a power law of the form $\langle\hbar\omega(q)\rangle \propto q^{1.80}$. When this expression is used in place of Dq^2 in Eq. (32) the scaling exponent u has the value 2.30 observed experimentally.

In our view this argues strongly that dipolar in-

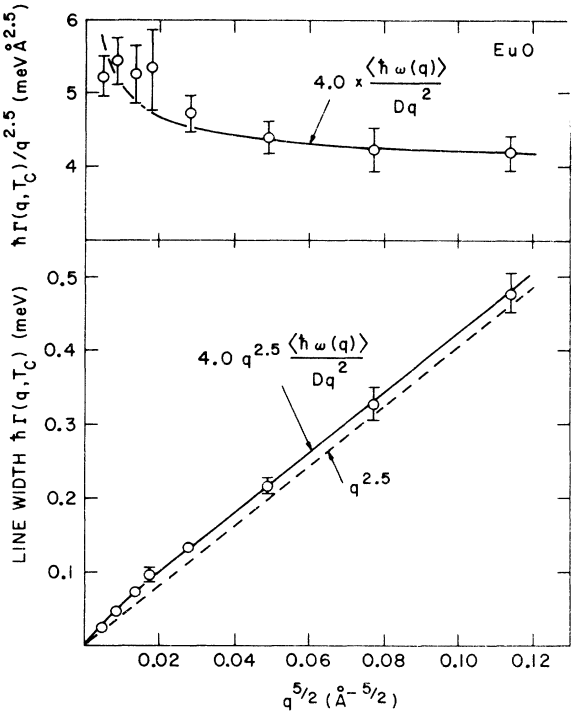

FIG. 11. Linewidth at T_C plotted vs $q^{5/2}$. Our results deviate from the $q^{5/2}$ law predicted by dynamical scaling (dashed line); the deviations at smaller values of q are particularly evident in the upper part of the figure which shows the linewidth divided by $q^{5/2}$. The solid lines represent the dynamic scaling behavior expected for an isotropic ferromagnet such as EuO when both dipolar and exchange interactions are taken into consideration. A discussion of how dynamical scaling predictions are modified by dipolar effects is given in Sec. V C 2.

teractions have an important influence on spin dynamics in EuO near T_C and must be taken into consideration whenever comparisons are made with theory. For the linewidths we can invoke the same scaling arguments used above to show that

$$\hbar\Gamma(q, T_C) = \sigma \mathcal{G}(0) q^{5/2} \langle \hbar\omega(q) \rangle / Dq^2 , \tag{34}$$

where the quantity $\langle \hbar\omega(q) \rangle / Dq^2$ represents the dipolar correction to the spin-wave energy, i.e., the coefficient of Dq^2 in Eq. (33), σ is the constant defined by Eq. (14), and $\mathcal{G}(0)$ is Hubbard's scaling function evaluated at $\kappa_1/q = 0$. The solid line in Fig. 11 is the best fit of Eq. (34) to the measured values of $\hbar\Gamma(q, T_C)$ obtained with $\sigma\mathcal{G}(0)$ treated as a parameter of the fit. Using this procedure, we found for $\sigma\mathcal{G}(0)$ a value of 4.0 ± 0.1 meV Å$^{5/2}$, which is almost 50% smaller than the value 6.4–7 meV Å^{-2} predicted by the theories outlined in Sec. II C.

We also measured $\hbar\Gamma(q, T_C)$ in EuS for $0.2 < q < 0.6$ Å^{-1} and found it to be three times smaller than in EuO. Both Riedel[42] and Hubbard[23] predict that

$$\frac{\hbar\Gamma(q, T_C)_{\mathrm{EuO}}}{\hbar\Gamma(q, T_C)_{\mathrm{EuS}}} = \left(\frac{a_{\mathrm{nn}}(\mathrm{EuO})}{a_{\mathrm{nn}}(\mathrm{EuS})} \right)^{5/2} \frac{T_C(\mathrm{EuO})}{T_C(\mathrm{EuS})} = 2.9 ,$$

(if we assume in applying Hubbard's theory that $J_1 + J_2$ is proportional to T_C). Thus, the ratio of the linewidths of EuO and EuS at T_C is properly given by the theory even though the predicted magnitudes are significantly larger than those observed experimentally.

D. Scaling function

Thus far we have used the dynamical scaling concept primarily to justify categorizing dynamic response according to whether q is larger or smaller than κ_1 and T is larger than, equal to or smaller than T_C. But, equally important, dynamical scaling also tells us that we can expect to obtain from the experimental data a scaling function which should serve as a means of consolidating observations extending over a wide range of wave vectors and temperatures into a single unified description of spin behavior.

According to Eq. (31), the normalized scaling function $\Omega(\kappa_1/q)/\Omega(0)$ is related to the normalized characteristic frequency $\hat{\omega}_q(\kappa_1)/\hat{\omega}_q(0)$ by the expression

$$\frac{\Omega(\kappa_1/q)}{\Omega(0)} = \frac{\hbar\hat{\omega}_q(\kappa_1)}{\hbar\hat{\omega}_q(0)} . \tag{35}$$

For the double Lorentzian spectral weight function of Eq. (24) it is easy to show that

$$\hbar\omega_q(\kappa_1) = [\,(\hbar\omega_q)^2 + (\hbar\Gamma)^2\,]^{1/2} , \tag{36a}$$

while for the single Lorentzian of Eq. (28)

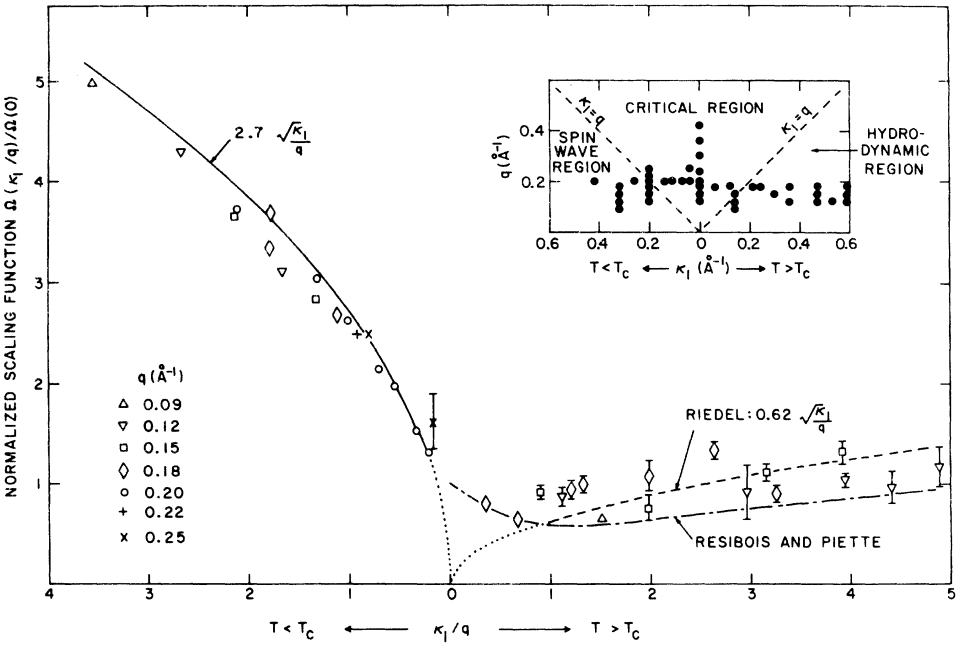

FIG. 12. Normalized dynamical scaling function $\Omega(\kappa_1/q)/\Omega(0)$ of EuO plotted against κ_1/q. All data from Tables I and II above 30 K are included in the figure. The inset indicates where on the $\kappa_1 - q$ plane the individual measurements were made. The dashed line represents the asymptotic form of $\Omega(\kappa_1/q)/\Omega(0)$ from Riedel's theory; the dash-dotted line is Rêsibois and Piette's scaling function.

$$\hbar\hat{\omega}_q(\kappa_1) = \hbar\Gamma \ .$$

Substituting from Tables I and III in the above equations and using Eq. (34) to define $\hbar\hat{\omega}_q(0)$ thus gives us directly $\Omega(\kappa_1/q)/\Omega(0)$. Figure 12 is a plot of the normalized scaling function obtained from all data above 30 K. As is evident, the concept of a single scaling function describing the dynamical response over a wide range of wave vectors and temperatures seems to be borne out remarkably well in practice.

In the inset to the figure we have shown where on the q-κ_1 plane the individual measurements were made. In addition, there is a dashed line to identify the traditional boundary between hydrodynamic and critical regimes. It also ought to be noted that dipolar interactions have little influence on the normalized scaling function (at least below T_C) because they affect the characteristic frequency below and at T_C in the same way.

From Eqs. (32), (34), and (35) it is easy to show that below T_C in the hydrodynamic limit $\kappa_1/q \gg 1$

$$\frac{\Omega(\kappa_1/q)}{\Omega(0)} \to \frac{W}{\sigma\mathcal{G}(0)}\left(\frac{\kappa_1}{q}\right)^{1/2} = W^-\left(\frac{\kappa_1}{q}\right)^{1/2} , \tag{37}$$

W being the constant defined in conjunction with Eq. (32). Using our experimental value 4.0 meV Å$^{5/2}$ for $\sigma\mathcal{G}(0)$ yields for W^- the value 2.7. Similarly, it follows from Eqs. (11), (35), and (36b) that in the hydrodynamic limit above T_C

$$\frac{\Omega(\kappa_1/q)}{\Omega(0)} \to \frac{3.3}{\sigma\mathcal{G}(0)}\left(\frac{a_{nn}}{F^+}\right)^{1/2}\left(\frac{\kappa_1}{q}\right)^{1/2} = W^+\left(\frac{\kappa_1}{q}\right)^{1/2} , \tag{38}$$

where a_{nn} is the nearest-neighbor distance and F^+ is the critical coefficient defined by the relation $a_{nn}\kappa_1 = F^+[(T - T_C)/T_C]^\nu$. The solid line in Fig. 12 is a plot of Eq. (37) with $W^- = 2.7$, while the dashed line represents Eq. (38) with $W^+ = 0.62$ corresponding to $\sigma\mathcal{G}(0) = 6.4$ meV Å$^{5/2}$, the value obtained from Riedel's calculation described in Sec. II C. Inspection of the figure shows that the hydrodynamic forms are satisfactory representations of the dynamic response over a large part of the $q - \kappa_1$ plane but fail, as would be expected, in the critical regime $q > \kappa_1$. Résibois and Piette's calculation of the scaling function above T_C[22]—appearing as the dash-dotted line in the figure—does, however, extend from the hydrodynamic into the critical regime and seems to satisfactorily reproduce the trend of the (limited) data in that region.

VI. DISCUSSION

It is obviously of interest to compare the asymptotic scaling functions of EuO with the equivalent functions for other isotropic ferromagnets. Accordingly, we have listed in Table V the values of the coefficients W^- and W^+ [defined by Eqs. (37) and (38)] for EuO together with values for iron, cobalt, and nickel derived from neutron data in the published literature. Inspection makes it immediately evident that W^- is about half as large for the metallic ferromagnets as for EuO while the values of W^+ fall reasonably close together.

TABLE V. Scaling functions of the isotropic ferromagnets in the hydrodynamic limit $\kappa_1/q \gg 1$, where $\Omega(\kappa_1/q) \to W^\pm(\kappa_1/q)^{1/2}$.

	$W^-(T < T_C)$	$W^+(T > T_C)$
EuO (This Expt.)	3.0(2.7) [a]	0.58(3)
Fe	1.51 [b]	0.43 [c]
Co [d]	1.50	0.47
Ni [f]		~0.77
Theory		0.43 [e]
		0.63 [f]

[a] The number in parentheses was obtained by using our experimental value 2.4 for the ratio F^-/F^+. All the other values of W^- were computed using the theoretical ratio 2.02 discussed in paper II.
[b] Reference 3.
[c] Reference 4.
[d] Reference 6.
[e] Reference 22.
[f] Reference 42.

We have not been able to derive from the existing theory any simple prediction as to how W^- might be expected to vary from one material to another. But it is easy to see from Eqs. (10), (14), and (38) that in the hydrodynamic limit W^+ should be proportional to $z^{-1/4}(a/a_{nn})^{1/2}$, where z is the number of nearest neighbors. For cubic lattices this quantity is independent of structure. Thus W^+ is expected to have about the same value for all isotropic ferromagnets. Keeping in mind that iron, cobalt, and nickel are not ideal Heisenberg ferromagnets and that much of the data used to estimate W^+ came from observations which were probably not made entirely within the hydrodynamic regime, the degree of consistency between experiments is better than might have been expected. Agreement with the value predicted by theory is also acceptable. Taken together, the measurements appear to support the view that the asymptotic scaling function above T_C is a universal quantity for isotropic ferromagnets.

Turning now to microscopic considerations, we find the neutron scattering cross section (discussed at length in Sec. V) adequately describes the inelastic magnetic scattering from EuO over a tem-

perature range extending from $0.14T_C$ to almost $2T_C$ and over a range of wave vectors from 0.09 Å^{-1} to essentially the Brillouin-zone boundary.

Our measurements below T_C indicate that spin-wave energies in EuO are well described by the Dyson[24]-Maleev[25] renormalization theory with the dynamical but not the kinematical interaction included. As long as the theory leads to self-consistent solutions (which it does at all temperatures below $0.9T_C$), the results are in good agreement with our observations. At approximately the temperature where the theory ceases to converge, we begin to see evidence of spin-wave broadening. To the limited extent that comparisons are possible, the temperature and wave-vector dependence of the observed linewidths appear to be consistent with the expectations of theory—the temperature dependence varying as $[(T-T_C)/T_C]^{-3\nu'/2}$ as predicted by Halperin and Hohenberg's dynamical scaling arguments[19] and the q dependence following the $\tilde{q}^4[\ln(2/\tilde{q}^2)]^2$ form predicted by Vaks, Larkin, and Pikin.[13] Also to be noted is the recent work of Raghavan and Huber[45] who not only predict the temperature and q dependence of the spin-wave linewidths, but also calculate their magnitudes with quite reasonable accuracy.

Looking at results below T_C from an over all point of view, we feel that the only important unresolved question is the form of $F^l(q,\omega)$—the longitudinal part of the spectral weight function. Here the theory of Vaks *et al.* predicts a three peaked function—a central diffusive peak and a pair of side peaks arising from the interaction of longitudinal spin fluctuations with long-wavelength propagating modes. Although our two-axis measurements show evidence of the contribution of longitudinal fluctuations to the scattering near T_C, we have not been able to find any indication of the expected central peak in our three-axis data. All of our results could be adequately represented by simply assuming $F^l(q,\omega)$ was identical to $F^t(q,\omega)$. Curiously, studies of other isotropic ferromagnets such as iron,[3] cobalt,[6] and nickel[7] led to the same conclusion which remains as yet unexplained by the theory.

Our investigations of spin diffusion in the hydrodynamic regime above T_C support the dynamical scaling prediction[19] that the diffusion coefficient Λ_T varies as $[\chi_{q=0}(T)/\chi_0]^{-1/4}$. Furthermore, the magnitude of Λ_T as predicted by theory[17,33] is in good agreement with our measurements.

We find that the $q^{5/2}$ dependence of the linewidths at T_C predicted by dynamical scaling[19] and observed in other isotropic ferromagnets[3,6,7] is slightly altered in EuO; the effective scaling exponent being reduced to 2.3. According to dynamical scaling, such a deviation would be expected if a significant part of the coupling between magnetic ions comes from dipolar interactions as is the case in EuO. Indeed, Maleev's recent analysis[46] of the influence of dipolar forces on critical spin dynamics in ferromagnets shows that the scaling exponent can be expected to "cross over" from $\frac{5}{2}$ to 1 as q falls below a certain value (estimated for EuO to be about 0.14 Å^{-1}), which is within the range covered by our measurements.

The magnitudes of the linewidths at T_C are about 50% smaller than the estimates of theory,[23,42] although the same theories correctly predict the linewidths of iron and nickel[42] as well as the width ratio for EuO and EuS. Oddly enough, the theory also overestimates the linewidth of the isotropic Heisenberg antiferromagnet $RbMnF_3$ by about the same amount as for EuO. Whether this discrepancy is simply an indication of the accuracy of mode-mode calculations or whether it represents a more fundamental difficulty with the theory remains as yet undetermined.

In summary, we find dynamical response in EuO in the hydrodynamic regime to be well described by the theory both above and below T_C. The main outstanding questions concern the magnitude of the linewidths at T_C and the interpretation of the longitudinal dynamical response near but below T_C. Finally, our studies show evidence (much of it indirect) of the influence of dipolar interactions on the dynamics of EuO not only at low temperatures but also in the critical regime both near and at T_C.

ACKNOWLEDGMENTS

We are grateful to M. Blume for several valuable comments, to M. Klenin for helping us find our way through some of the more arcane points of dynamical theory, and to P. Résibois and M. de Leener for helpful discussions of their work. Also, we are obligated to P. Bak for exploring on our behalf several problems encountered with the interpretation of the theory and to D. L. Huber for much useful advice and for sending us the results of calculations made by himself and R. Raghavan in advance of publication. Finally, we wish to express our appreciation to W. Kunnmann and M. Shafer for preparing the EuO samples used in these experiments.

†Research sponsored by the U. S. Energy Research and Development Administration.

*Part of the work done while a Guest Scientist at Brookhaven National Laboratory.

[1]C. G. Windsor, Proc. Phys. Soc. (Lond.) 89, 825 (1966).
[2]A. Tucciarone, H. Y. Lau, L. M. Corliss, A. Delapalme, and J. M. Hastings, Phys. Rev. B 4, 3206 (1971).
[3]M. F. Collins, R. Nathans, L. Passell, and G. Shirane, Phys. Rev. 179, 417 (1969).
[4]R. Kahn and G. Parette, J. Phys. (Paris) 32, C1-523 (1971).
[5]S. Boronkay and M. F. Collins, Int. J. Magn. 4, 205 (1973).
[6]C. J. Glinka, V. J. Minkiewicz, and L. Passell, AIP Conf. Proc. 24, 283 (1975).
[7]V. J. Minkiewicz, M. F. Collins, R. Nathans, and G. Shirane, Phys. Rev. 182, 624 (1969).
[8]H. A. Mook, J. W. Lynn, and R. M. Nicklow, AIP Conf. Proc. 18, 781 (1974).
[9]E. J. Samuelsen, R. Silberglitt, G. Shirane, and J. P. Remeika, Phys. Rev. B 3, 157 (1971).
[10]V. J. Minkiewicz, K. Gesi, and E. Hirahara, J. Appl. Phys. 42, 1374 (1971).
[11]L. Passell, J. Als-Nielsen, and O. W. Dietrich, in *Proceedings of the Fifth IAEA Symposium on Neutron Inelastic Scattering* (International Atomic Energy Agency, Vienna, 1972), p. 619.
[12]C. J. Glinka, V. J. Minkiewicz, and L. Passell, AIP Conf. Proc. 18, 1060 (1973).
[13]V. G. Vaks, A. I. Larkin, and S. A. Pikin, Zh. Eksp. Teor. Fiz. 53, 1089 (1967) [Sov. Phys.-JETP 26, 647 (1968)].
[14]F. Keffer, in *Encyclopedia of Physics* (Springer-Verlag, Berlin, 1966), Vol. XVIII/2, p. 1.
[15]P. G. de Gennes, J. Phys. Chem. Solids 4, 223 (1958).
[16]H. Mori and K. Kawasaki, Proc. Theor. Phys. 27, 529 (1962).
[17]H. S. Bennett and P. C. Martin, Phys. Rev. 138, A608 (1965).
[18]M. Månson and A. Sjöllander, Phys. Rev. B 11, 4639 (1975).
[19]B. I. Halperin and P. C. Hohenberg, Phys. Rev. 177, 952 (1969).
[20]B. Widom, J. Chem. Phys. 43, 3892 (1965); 43, 3898 (1965).
[21]L. P. Kadanoff, Physics (N.Y.) 2, 263 (1966).
[22]P. Résibois and C. Piette, Phys. Rev. Lett. 24, 514 (1970).
[23]J. Hubbard, J. Phys. C 4, 53 (1971).
[24]F. J. Dyson, Phys. Rev. 102, 1217 (1956); 102, 1230 (1956).
[25]S. V. Maleev, Zh. Eksp. Teor. Fiz. 34, 1518 (1958) [Sov. Phys.-JETP 7, 1048 (1958)].
[26]W. Marshall and S. W. Lovesey, *Theory of Thermal Neutron Scattering* (Oxford U. P., London, 1971).
[27]F. Keffer and R. Loudin, J. Appl. Phys. 32, 25 (1961).
[28]J. F. Cooke and H. A. Gersch, Phys. Rev. 152, 641 (1967).
[29]A. B. Harris, Phys. Rev. 175, 674 (1968); 184, 606 (1969).
[30]B. I. Halperin and P. C. Hohenberg, Phys. Rev. 188, 898 (1969).
[31]L. van Hove, Phys. Rev. 95, 1374 (1954).
[32]M. F. Collins and W. Marshall, Proc. Phys. Soc. (Lond.) 92, 390 (1967).
[33]K. Kawasaki, J. Phys. Chem. Solids 28, 1277 (1967).
[34]This expression is given by D. L. Huber [J. Phys. Chem. Solids 32, 2145(1971)].
[35]D. S. Ritchie and M. E. Fisher, Phys. Rev. B 5, 2668 (1972).
[36]K. Kawasaki, Prog. Theor. Phys. 39, 285 (1968).
[37]F. Wegner, Z. Phys. 216, 433 (1968).
[38]M. de Leener and P. Résibois, Phys. Rev. 178, 819 (1969).
[39]M. Blume and J. Hubbard, Phys. Rev. B 1, 3815 (1970).
[40]G. F. Reiter, Phys. Rev. B 5, 222 (1972).
[41]H. Mori, Prog. Theor. Phys. 33, 423 (1965).
[42]E. K. Riedel, J. Appl. Phys. 42, 1383 (1971).
[43]Y. Shapira and T. B. Reed, J. Appl. Phys. 40, 1197 (1969).
[44]M. Nielsen and H. Bjerrum Møller, Acta Crystallogr. A 25, 547 (1969).
[45]R. Raghavan and D. L. Huber, Phys. Rev. B (to be published).
[46]S. V. Maleev, Zh. Eksp. Teor. Fiz. 66, 1809 (1974) [Sov. Phys.-JETP 39, 889 (1974)].